

SMART WATER RECEIVER FOR USE IN THE WET PRESS SECTION OF A
PAPER MACHINE

A Thesis
Presented to
The Academic Faculty

By
Wyly Gilfoil

In Partial Fulfillment
Of the Requirements for the Degree
Master of Science in Mechanical Engineering

Georgia Institute of Technology

August 2005

SMART WATER RECEIVER FOR USE IN THE WET PRESS SECTION OF A
PAPER MACHINE

Approved by:

Dr. David I. Orloff, Advisor
School of Mechanical Engineering
Georgia Institute of Technology

Dr. Dr. Timothy Patterson
School of Mechanical Engineering
Georgia Institute of Technology

Dr. Dr. Frederick W. Ahrens
School of Mechanical Engineering
Georgia Institute of Technology

Date Approved: May 6, 2005

ACKNOWLEDGEMENT

First and foremost, I would like to thank Dr. David Orloff for his guidance and helping hand throughout this project. When Dr. Orloff and I first discussed the project, he said that his overarching goal in all of his projects was to help his students learn. I believe he has succeeded in that with this project.

I would like to thank Dr. Fred Ahrens and Dr. Tim Patterson for serving on my committee and for the input they have given to this project. I also owe gratitude to Isaak Rudman and Roman Popil for their insight, especially when problems arose, into the project. My thanks to Marion Pena for her kindness and help. Finally, I would like to thank Mark Urbin and Perry Arrington for their help in manufacturing and obtaining the supplies I needed to complete experimentation.

TABLE OF CONTENTS

ACKNOWLEDGEMENTS	iii
LIST OF TABLES	vi
LIST OF FIGURES	viii
LIST OF SYMBOLS	xi
SUMMARY	xii
CHAPTER 1 INTRODUCTION	1
1.1 Project Purpose	1
1.2 Project Background	1
1.3 Project Methodology	2
CHAPTER 2 LITERATURE REVIEW	6
2.1 Rewet	6
2.2 Patent Review	11
2.3 Computer Modeling of Smart Felt	19
CHAPTER 3 METHODOLOGY	29
3.1 Design of Smart Water Receiver Prototype	29
3.2 Design of Experimental Apparatus	39
3.3 Experimental Procedure	44
CHAPTER 4 RESULTS AND DISCUSSION	48
CHAPTER 5 CONCLUSIONS AND RECOMMENDATIONS FOR FUTURE WORK	57
APPENDIX A: RAW DATA	60
A.1 Calibration Data	61

A.2 Entrance Length Calculations	63
A.3 Extrapolation for Determination of Angle of Deflection	63
APPENDIX B: EXPERIMENTAL RESULTS	64
APPENDIX C: UNCERTAINTY ANALYSIS	70
APPENDIX D: DIMENSIONED DRAWINGS OF PROTOTYPE	74
APPENDIX E: EQUIPMENT SPECIFICATIONS	79
E.1 Flowmeter Specifications	80
E.2 Thermocouple Specifications	81
E.3 Manometer Specifications	82
APPENDIX F: MATERIAL PROPERTIES OF ACETRON GP	83
APPENDIX G: REYNOLDS NUMBER AND GEOMETRIC SCALING	86
REFERENCES	89

LIST OF TABLES

Table

3.1:	Cantilever Dimensions for Valves Used in Micro-Fluidic Systems	30
3.2:	Cantilever Beam Dimensions for Valves in Smart Valve Layer	30
3.3:	Dimensions of Cantilever Beam for Valve Prototype	31
3.4:	Mechanical Properties of Acetron GP Acetal	33
3.5:	ΔP Required to Deflect Cantilever by Angle θ for Acetron GP	40
A.1:	Calibration Data for Measured Calibration of FLR 1012	61
A.2:	Factory Calibration Data for FLR 1012	61
A.3:	Constants	63
A.4:	Entry Length Calculations	63
A.5:	Projection from Figure 4.10 with Intercept at Zero	63
B.1:	Reynolds Number Results for No Pins in Prototype	65
B.2:	Reynolds Number Results for Pin 1 in Prototype	67
B.3:	Reynolds Number Results for Pin 2 in Prototype	68
B.4:	Reynolds Number Results for Pin 3 in Prototype	69
C.1:	Flow Measurement Uncertainty Summary	73
C.2:	Pressure and Diameter Measurement Uncertainty Summary	73
C.3:	Loss Coefficient Uncertainty Summary	73
C.4:	Reynolds Number Uncertainty Summary	73
E.1:	Manometer Specs for 3986K14	82
F.1:	Material Properties of Acetron GP Acetal	84

LIST OF FIGURES

Figure		
1.1:	(a) Closed Valve and (b) Open Valve	3
2.1:	Representation of Patent 3,840,429	11
2.2:	Representation of Patent 4,588,475	12
2.3:	(a) Representation of Patent 6,616,812, (b) Alternative Embodiment of Patent 6,616,812	13
2.4:	(a) Representation of Patent 5,372,876, (b) Flow-Control Layer	14
2.5:	Representation of Patent 4,162,190	15
2.6:	Representation of Patent 6,592,636	16
2.7:	Representation of Patent 5,204,171	16
2.8:	Representation of Patent 5,232,768	17
2.9:	Representation of Patent 4,988,409 – (a) Initial State of Web and Felt Prior to Nip (b) Compressed State of Web and Felt, (c) Expanded State of Web and Felt	18
2.10:	Representation of Patent 4,199,401	19
2.11:	Outgoing Solids and Ratio of Expansion-to-Compression Water vs. Nip Time	21
2.12:	Outgoing Solids and Ratio of Expansion-to-Compression Water vs. Permeability of Smart Felt	22
2.13:	Water Velocity at Sheet/Felt Interface and Felt Permeability vs. Nip Time	23
2.14:	Outgoing Solids, Ratio of Expansion-to-Compression Water, and Hydraulic Pressure vs. Sheet-Side Batt Basis Weight	24
2.15:	Outgoing Solids, Ratio of Expansion-to-Compression Water, and Hydraulic Pressure vs. Sheet-Side Batt Permeability	25

2.16:	Domain of 2-D, 2-Zone Smart Felt Simulation	26
2.17:	Outgoing Solids and Hydraulic Pressure vs. Valve Opening	27
2.18:	Outgoing Solids and Non-uniformity of Water Removal vs. Valve Opening for Various Basis Sheet-Side Batt Basis Weights	28
3.1:	Valve Configuration in Smart Felt	34
3.2:	(a) Solid Side View of Valve Prototype, (b) Solid Bottom Isometric View, I Solid Top Isometric View	37
3.3:	3-D Wireframe View of Valve Prototype	38
3.4:	Valve Prototype	38
3.5:	Rear View of Pins Placed in Prototype	39
3.6:	Experimental System	41
3.7:	Experimental System Photograph	42
3.8:	Flow Meter, Regulating Valve and Water Filter	42
3.9:	Thermocouple	43
3.10:	Manometer	43
4.1:	Flow Rate vs. Pressure Drop with No Pins in the Prototype	48
4.2:	Loss Coefficient vs. Reynolds Number with No Pins in the Prototype	49
4.3:	Flow Rate vs. Pressure Drop Comparison for Pin 1	50
4.4:	Loss Coefficient vs. Reynolds Number Comparison for Pin 1	51
4.5:	Flow Rate vs. Pressure Drop Comparison for Pin 2	52
4.6:	Loss Coefficient vs. Reynolds Number Comparison for Pin 2	52
4.7:	Flow Rate vs. Pressure Drop Comparison for Pin 3	53
4.8:	Loss Coefficient vs. Reynolds Number Comparison for Pin 3	54
4.9:	Angle vs. Pressure Drop for Cantilever Beam	55

4.10:	Angle vs. Velocity for Cantilever Beam	55
5.1:	Sample Valve Layer for Experimentation in MTS Press	59
A.1:	Calibration Curve for Measured Calibration of FLR 1012	61
A.2:	Factory Calibration Curve for FLR 1012	62
D.1:	Dimensions for Top Layer of Valve Prototype	75
D.2:	Section View of Prototype	75
D.3:	Section A-A View of Prototype	76
D.4:	Section B-B View of Prototype	77
D.5:	Dimensions for Bottom Layer of Prototype	78
E.1:	Flow Meter Specs for FLR 1012	80
E.2:	Thermocouple Specs for TC-J-NPT	81
G.1:	(a) Unit Cell for Smart Valve Layer, (b) Valve Prototype	87

LIST OF SYMBOLS (IN ORDER OF APPEARANCE)

$\delta(x)$	deflection of cantilever beam	m	non-dimensional transversal mass coordinate
W	Force per unit length	R_h	radius of valve opening
x	position in the horizontal direction	R	total radius of the valve
E	Young's modulus	P_h	hydraulic pressure
I	moment of inertia	t	thickness
l	length in horizontal direction	σ_{\max}	maximum stress
θ	angle of deflection	a	length of side of square
ΔP	pressure difference	Re	Reynolds number
V	velocity	D_h	hydraulic diameter
μ	viscosity	w	width
L	length in thickness direction	$u_{N,y}$	Nth order uncertainty for y
K	permeability	y	quantity being measured
ρ	density	u	uncertainty
K_L	loss coefficient	u_o	1/2 resolution of instrument
P_s	structural pressure	R	result of calculation
N	empirical parameter	θ_i	partial derivative of R with respect to y_i
c_o	ingoing apparent density	u_{y_i}	uncertainty in quantity y
M	empirical parameter	Q	flow rate
c	compressibility	D	diameter

SUMMARY

When the paper web and press felt enter a nip in the press section of a paper machine, both the paper web and felt are compressed. Water is forced from the paper sheet into the press felt due to a hydrodynamic pressure gradient between the sheet and felt. Water enters the uppermost batt layer of the felt and continues into the void volume of the base fabric of the felt. Some of the water then leaves the felt and enters grooves in the press roll, while some water remains in the felt. Water not only flows through the felt in the transversal z-direction, but also flows through the felt in the machine and cross-machine directions.

On the exit side of the nip, the pressure imposed on the sheet-felt system by the rolls begins to decrease. Both the paper web and press felt begin to expand, and a vacuum is created in the web and felt. The vacuum in the web is stronger than that in the felt, and thus water and air tend to flow from the felt back into the sheet, causing rewet. Three mechanisms that contribute to rewet have been proposed: 1) film splitting between the paper web and press felt, 2) capillary forces in the web drawing water from the felt into the web, and 3) the pressure differential between the web and felt during expansion. Numerous alterations of the press felt have been made in an attempt to reduce the rewet of the paper web up on exit from the press nip.

The objective of this project was to design and test under flow conditions similar to those in a press nip a “smart” water receiver to be used in the press section of a paper machine. In this manner, the feasibility of such a water receiver was to be determined. The purpose of this water receiver is to accept water that is pressed from the paper web in

a nip and prevent the return of this water to the paper web upon exit from the nip. Thus, the smart water receiver allows flow through the felt in the positive z-direction of the felt (away from the paper web) and not in the negative z-direction (towards the paper web). The smart water receiver concept utilizes a layer of micro-check valves incorporated into the press felt to perform in the desired manner. A mathematical model and lab-scale prototype were created in order to predict the behavior of such a design in the press nip.

CHAPTER 1

INTRODUCTION

1.1 Project Purpose

The concept of a smart water receiver pertains to the wet press felt in the press section of a paper machine. Inherent in this concept is the ability of the water receiver to display different properties under varying environmental conditions such as temperature or pressure. The focus of this project is to design and characterize the behavior of a smart water receiver that minimizes rewet.

1.2 Project Background

When the paper web and press felt enter a nip of the press section, both the paper web and felt are compressed. Water is forced from the paper sheet into the press felt due to a hydrodynamic pressure gradient between the sheet and felt. Water enters the uppermost batt layer of the felt and continues into the void volume of the base fabric of the felt. Some of the water then leaves the felt and enters grooves in the press roll, while some water remains in the felt. Upon exiting the press nip, water returns from the press felt to the paper web. This phenomenon is known as rewet.

In the paper industry, three mechanisms are widely accepted as the cause of rewet: 1) film splitting between the paper web and press felt, 2) capillary forces in the web drawing water from the felt into the web, and 3) the pressure differential between the web and felt during expansion. In this project, the latter two causes are addressed. In

researching the patent literature, no existing patents were found that have had commercial success in preventing rewet due to these mechanisms.

The prevention of rewet offers several advantages in paper production, among which are the following (Yli-Kauppila and Valmet 31):

- Increased production rates
- Energy consumption in the dryer section can be decreased
- Less requirement on dryer section means reduction in size and cost of dryer section

For every percentage point gain in dryness in the press section, a 4% gain in energy savings can be realized in the dryer section (Bermond 901).

1.3 Project Methodology

The design to be employed in the smart water receiver is similar to micro check valves, shown in Figure 1.1 (Hok et al 391), that are employed in micro-pumps used for ink-jet printing and drug delivery in biomedical applications. The smart water receiver, conceptually, consists of a layer of multiple flexible cantilever beams that act as swing check valves, and thus alter the permeability of the press felt under varying pressure gradients across the valve. The pressure differential between the paper web and the felt will, theoretically, force the valve shut to prevent water from flowing from the felt to the web upon expansion of the web. The capillary attraction between the water in the web and water in the felt will be broken upon closing of the valve. The equation that governs the deflection of a cantilever beam is given below in Equation 1.1 (Orthwein 134), and the angle of deflection is given in Equation 1.2 (Orthwein 134).

$$\delta(x) = \frac{Wx^2}{24EI} [x^2 - 4lx + 6l^2] \quad (1.1)$$

$$\theta = \frac{Wl^3}{6EI} \quad (1.2)$$

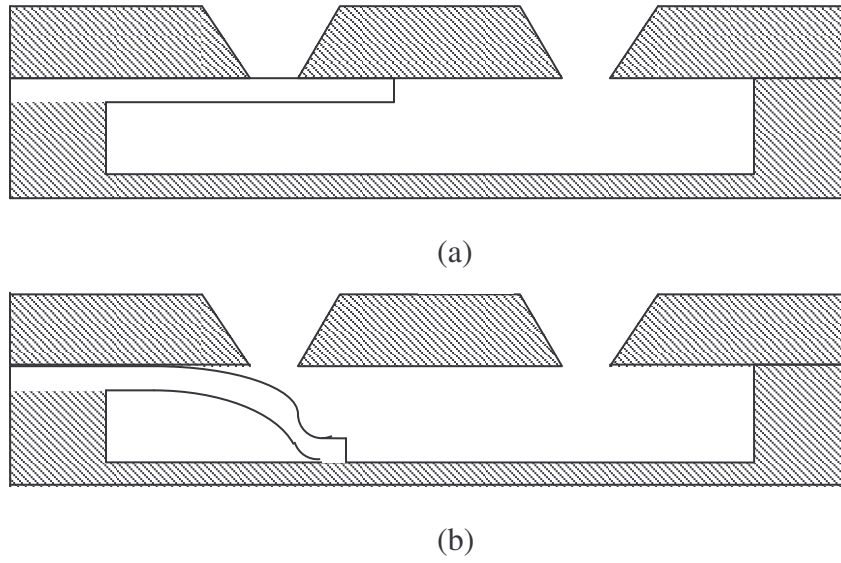


Figure 1.1: (a) Closed Valve and (b) Open Valve

In order to predict the behavior and performance of the valve layer in a press nip, a computer model (developed in an AMRC project, Fundamental Model of Wet Pressing) and experiments on a prototype of the valve layer were utilized. The computer model requires an approximation of the permeability of the valve layer in order to predict its performance. A first approximation of this permeability was obtained using Darcy's Law, as given in Equation 1.3 (Greenkorn 3).

$$\Delta P = \frac{V\mu L}{K} \quad (1.3)$$

To find K , the velocity and pressure drop must be known. The velocity can be estimated by assuming a change in percent solids of the paper sheet over a specified time in the nip. The velocity is then related to the pressure drop by the following equation, Equation 1.4 (Blevins 87).

$$\frac{\rho}{2}(K_L)V^2 = \Delta P \quad (1.4)$$

K_L in Equation 1.4 represents the loss coefficient of the valve, not permeability. This loss coefficient was estimated by combining the contraction coefficient of a nozzle with loss coefficients for swing check valves obtained from Blevins (87). The permeability can be found with knowledge of the pressure drop and velocity. Upon substituting the initial results of the permeability calculations into the computer model and assuming a lightweight paper web, the valve layer increased the percent solids of the paper web on the outgoing side of the nip by 2.6% over a conventional felt (Rudman 8-24-04).

In order to more accurately predict the performance of the valve using the computer model and to study the behavior of the valve layer, an experimental setup was constructed. In this setup, an enlarged prototype of the valve layer was placed between two pipe flanges in a PVC pipe. The flow rate of water through the pipe, the temperature and the pressure drop across the valve were measured. The behavior of the valve layer

was studied to determine the flow rate required to open the valve, the angle of opening of the valve, and the pressure drop associated with this valve opening angle. The measurement of the pressure drop across and flow rate through the valve allowed for a better prediction of the loss coefficient to be employed in calculating the valve permeability for the computer model. The feasibility of the utilization of a valve layer in a press felt was analyzed by comparing the Reynolds number of flow in experimentation to common Reynolds numbers in a press nip.

CHAPTER 2

LITERATURE REVIEW

2.1 Rewet

The press felt serves several purposes in the press section of a paper machine.

Among these are:

- Transferring the paper sheet through the press section
- Dewatering the paper sheet
- Serving as a drive belt for non-driven rolls in the paper machine
- Bridging holes present in grooved and suction rolls
- Providing a finish to the paper sheet
- Providing uniform pressure distribution over the paper sheet

The current study is primarily concerned with changing the press felt to improve the dewatering performance of the paper sheet. Although press clothing costs account for less than 5% (Shaw 59) of the total paper manufacturing costs, extensive savings can be realized through improved felt properties. For every percentage point gain in dryness in the press section, a 4% energy savings can be generated in the steam drying section of the paper machine. This stems from the ratio of energy used in the dryer section to energy used in the press section, which is 15:1 (Bermond 901). As long as the durability of the press felt is not decreased significantly, altering its properties to improve sheet dryness is the most economical method of improving wet pressing because of the relatively low cost of the press felt.

Dewatering of the paper web is influenced by several factors in the press nip. Among these are the compressive pressure in the nip, the machine speed, the properties of the paper web, and the properties of the press felt. Total pressure in the nip is a combination of the structural pressure and hydraulic pressure of water in the sheet and felt. The mechanical pressure applied by the press rolls is resisted by structural pressure in the felt and paper fibers and hydraulic pressure from water in the nip. A hydraulic pressure gradient causes the water to flow from the sheet into the felt. Generally, higher press loadings increase the amount of water removed from the paper web, while increased machine speed decreases water removal due to the paper web spending less time in the press nip. However, at low machine speeds, the paper web is in contact with the press felt longer than at high machine speeds. This can lead to increased rewet of the paper web.

In order for rewet to occur, two conditions must be met:

1. Water must be present in the interfacial region between the paper web and the press felt.
2. A driving force must be present to move the water from the felt back into the paper web (Ibrahim 46).

Although the amount that each contributes is disagreed upon, three driving forces are accepted as the cause of rewet. These forces are:

1. capillary action
2. mechanical absorption
3. film splitting

Capillary attraction is a combination of adhesion, cohesion and surface tension. The paper sheet has finer, narrower capillaries than the press felt, and thus the paper web generates more capillary force than the press felt. Mechanical absorption of water by the web occurs because of the difference in vacuum between sheet and felt upon expansion. The paper web creates a stronger vacuum, from 60 (Szikla 164) to 90 kPa (Palokangas 103), upon expansion than does the press felt, which has a vacuum of approximately 40 kPa (Szikla 164). Water is therefore sucked from the felt into the web on the expanding side of the nip. Film splitting occurs when the felt and sheet are separated. The thin film of water in the interfacial region between the felt and sheet is split between the felt and sheet. The amount of water split between the sheet and felt is dependent upon the surface properties of each. These driving forces have less of an effect when the contact time between the paper web and felt is reduced.

Properties of the press felt and the paper web both have an effect on the amount of rewet that occurs due to the driving forces described above. The degree to which these properties affect the dewatering of the paper web and rewet is widely debated.

Press nips can be either flow controlled or pressure controlled. Pressure controlled nips occur primarily for lower weight sheets. In pressure controlled nips, the paper sheet does not offer significant flow resistance to water leaving the web. The amount of water removed is dependent on the uniformity of pressure applied to the sheet and the amount of rewet. Flow controlled nips occur for higher weight paper sheets. In these sheets, the pores offer significant resistance to water flow and cause a buildup of hydraulic pressure in the web. Rewet tends to be more of a factor in pressure controlled nips because the water that flows back into the paper web upon expansion and exit from

the nip constitutes a higher percentage of the basis weight of the sheet. Rewet is generally regarded as a surface effect determined by the surface-to-volume ratio of the paper sheet. For low basis weight sheets, the surface-to-volume ratio is high, thus rewet plays a more important role in pressing these sheets.

The degree to which pressure uniformity and rewet contribute to the solids content of the paper sheet is disputed. The properties of the felt which increase the former decrease the latter. Fitton proposes that decreasing the diameter of the batt fiber in contact with the sheet increases water removal by creating a more uniform pressure distribution for the paper web (51). Decreasing the diameter of the batt fiber also allows the batt fibers to be more tightly packed. This creates more capillary attraction in the felt, which reduces the amount of rewet by countering the capillary attraction of the paper web upon exiting the nip. Szikla states that “the micro-scale uniformity of pressure application has a relatively small effect, significantly smaller than so far expected, on the water removal (160).” Rewetting, then, would be the major determining factor on the moisture content of the exiting paper web, and indeed, Wilder suggests that up to 50% of the water removed in compression returns during expansion of the paper web (104). Ceckler, et al, agrees that rewet plays an important role, but asserts that only up to 30% of water removed from the paper web is returned by rewetting (151).

According to Wahlstrom, the felt has a passive role on the ingoing portion of the nip if it provides uniform pressure distribution to the paper sheet and little flow resistance (in Smart 172). On the expansion side of the press nip, the felt plays an active role because of the influence of rewet.

Felt performance is dictated by four key factors (Plaisted 42):

1. The void volume available in the felt – The press felt must have adequate space to accept water pressed from the paper web.
2. The felt's compression/relaxation properties – The press felt should be able to withstand repeated loadings and still return to near its original volume.
3. The felt's flow resistance in compression – The felt must provide minimal flow resistance in compression to avoid crushing of the sheet due to the build-up of hydraulic pressure. The permeability of the felt must be high enough to allow water to pass through. However, felts with closely packed batt fibers are desirable in reducing rewet because of their capillary structure.
4. The moisture content of the felt – The effect of moisture content is disputed. In some situations, the moisture content plays a crucial role in sheet solids, while in others, it has no effect. For instance, Wiseman found that felt moisture content affects sheet solids at low machine speeds. Felt moisture content can be important to flow resistance and the buildup of hydraulic pressure. This is important for plain roll presses more so than vertical, grooved roll presses. In plain roll presses, space must be available to accept water from the sheet. The moisture content of the felt also affects the distribution of capillary pressure in the press section (29-33).

Properties such as durability and cleanability of the felt also affect the dewatering of the paper sheet. These properties affect the permeability of the felt, which in turn plays a role in the amount of water removed from the web.

2.2 Patent Review

Numerous alterations of the press felt have been made in an attempt to reduce the rewet of the paper web upon exit from a press nip. The following patents are among these attempts.

Patents 3,840,429; 4,588,475; and 6,616,812 each utilize the concept of rapid separation between the sheet and the press felt to minimize rewet. In patents 5,372,876; 4,162,190 and 6,592,636, flow control layers are used to prevent rewet. High flow resistance in the z-direction is utilized in patent 5,204,171 and 5,232,768. Patents 4,988,409 and 4,199,401 incorporate stratification of the felt to reduce rewet.

In patent 3,840,429, an extended nip with a flow-resistant layer, shown in Figure 2.1, between the web and felt is employed. The flow-resistant layer could be a material such as porous stainless steel or plastic. Pressure is applied to the felt in a pressure chamber using liquid pressure supply lines. The web spends a much longer time in compression than in expansion, and thus water has time to flow through the flow-resistant layer in compression, but does not have the opportunity to return to the web through the flow-resistant layer during expansion because of the quick separation time.

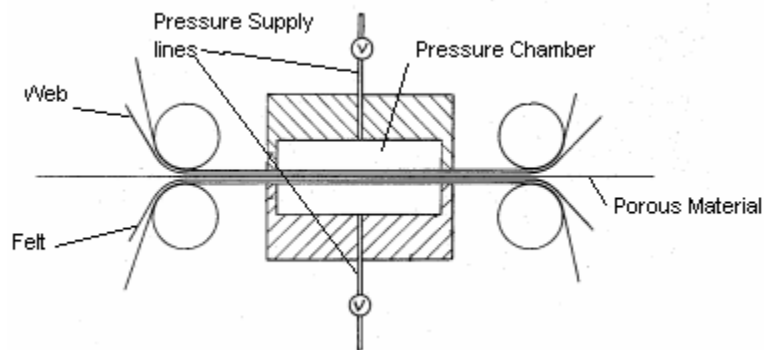


Figure 2.1: Representation of Patent 3,840,429 (Busker and Daane)

In patent 4,588,475 (shown in Figure 2.2), passing a water-impermeable layer through the nip with one surface in contact with the paper web is proposed. The mat is kept in tension by a second set of rolls so that it does not expand to its original volume after the press nip, and thus the compressive stress decreases rapidly after the centerline of the nip. The press felt is therefore not held in contact with the paper web after the centerline of the nip. The mat provides a method for separating the web from the felt shortly after the nip, so that rewet is minimized.

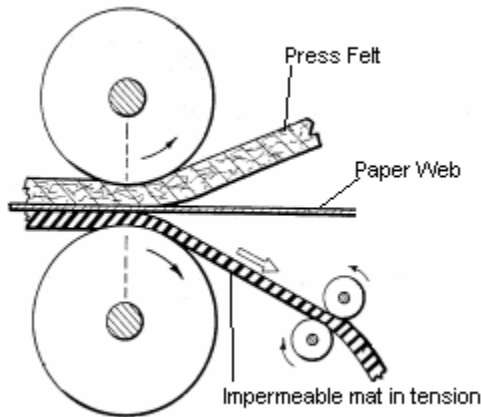


Figure 2.2: Representation of Patent 4,588,475 (Lundstrom)

Patent 6,616,812, depicted in Figure 2.3, pertains to a felt used in an air press. In an air press, mechanical pressure from press rolls is complimented by fluid pressure in a pressure chamber. A perforated film is placed on the underside of the air distribution layer of the press felt. Water is forced from the paper web by air pressure and is deposited on the press roll side of the perforated film layer, facing away from the paper web. Upon exit from the press nip, air flow separates the web from the press felt. Capillary forces, therefore, cannot attract water back into the paper web, and rewet is

minimized. Figure 2.3(a) shows a felt with one air distribution layer attached to the perforated film, while Figure 2.3(b) is an alternative embodiment with two air distribution layers attached to the perforated film.

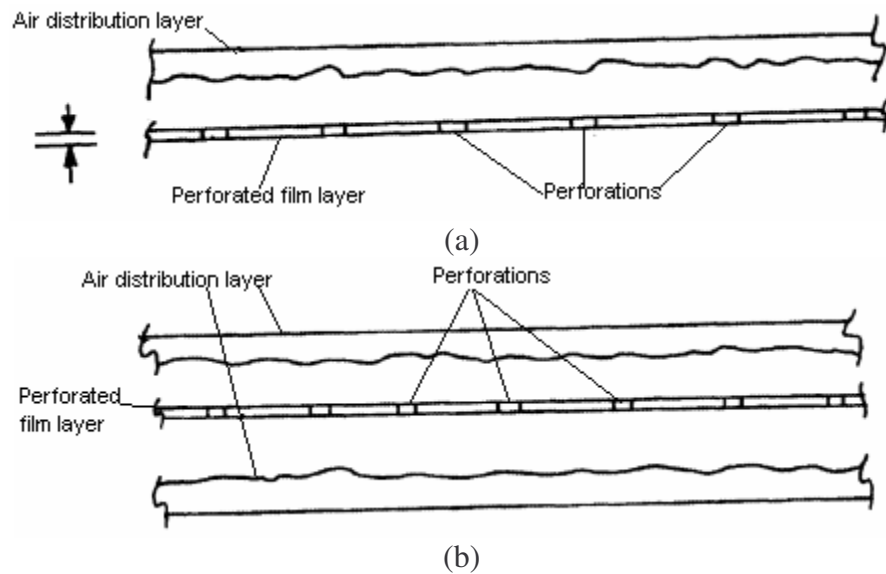
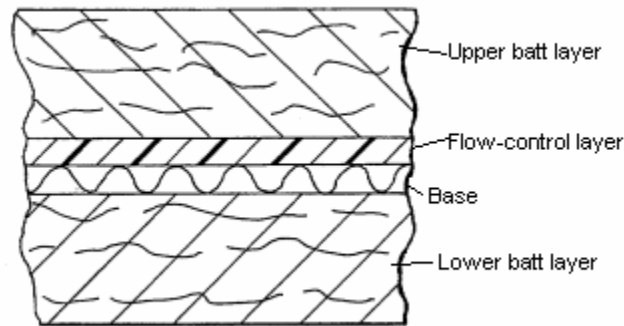
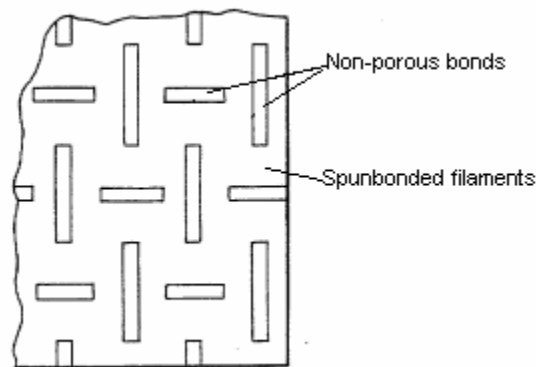


Figure 2.3: (a) Representation of Patent 6,616,812, (b) Alternative Embodiment of Patent 6,616,812 (Beck)

A porous hydrophobic material is placed between the base and batt layer of the press felt in patent 5,372,876 (illustrated in Figure 2.4 on the following page). The batt, base, and flow-control layers are joined together through a needling process. The flow-control layer is preferably a spunbonded nylon material which is rendered hydrophobic through chemical coating. The individual filaments of the flow-control layer are bonded in the pattern shown in Figure 2.4(b). Water is forced through the layer under pressure in the press nip, but the hydrophobicity of the flow control layer prevents backflow of water when pressure is relieved.



(a)



(b)

Figure 2.4: (a) Representation of Patent 5,372,876, (b) Flow-Control Layer (Johnson and Schultz)

In patent 4,162,190 (shown in Figure 2.5), a hydrophobic layer is incorporated into the felt. This layer may be composed of hydrophobic material or chemically coated to obtain its hydrophobic properties. This hydrophobic layer is in contact with the paper web in the press nip, and is attached to a hydrophilic, or less hydrophobic, layer by a needling process, adhesives, or binders. This hydrophilic layer is then attached to a woven base. Water is pressed through the hydrophobic layer into the less hydrophobic layer of the felt. The water does not return to the paper web because of the hydrophobic properties of the upper layer of the felt. The surface layer of the felt is composed of fine

fibers, while more coarse fibers are beneath the surface layer. This, in theory, reduces the capillary attraction of water to the paper web upon exiting the press nip.

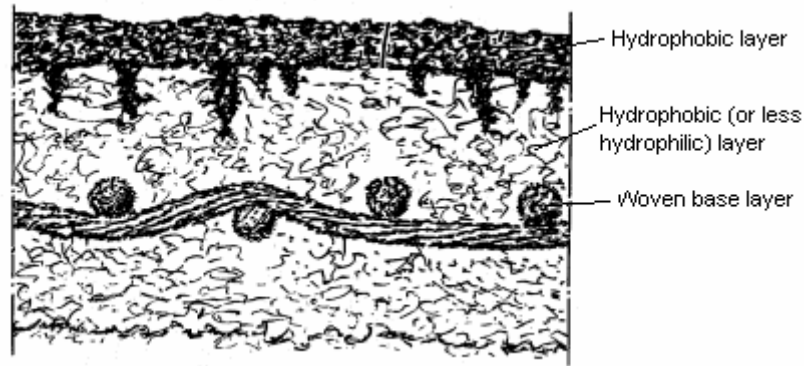


Figure 2.5: Representation of Patent 4,162,190 (Ashworth)

In patent 6,592,636 (illustrated in Figure 2.6), a fused batt layer is proposed to prevent water from returning to the web. Two to three batt applications are needled into the base layer of the felt. The felt then undergoes a \square alendar \square ng process, where heat and pressure are applied to the batt. The temperature in the \square alendar nip is above the melting point of the fiber batt. The felt is then immediately cooled so that the fiber batt layer is fused. A hydrophilic coating may also be applied to this batt layer. Additional batt layers can then be needled into the fused layer. The fused batt layer serves as a barrier to water returning to the paper web upon exiting the nip. Water is forced through this layer under pressure in the nip. When pressure is relieved, the fused layer prevents water from returning to the paper web. The hydrophilic treatment also attracts water to the barrier layer to prevent rewet. The barrier layer can be located anywhere within press felt.

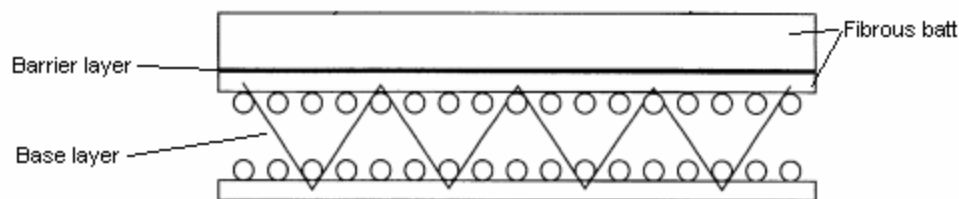


Figure 2.6: Representation of Patent 6,592,636 (Joyce)

A blocking layer, shown in Figure 2.7, is placed in the press felt in patent 5,204,171. This layer covers 45-85% of the flow cross-section of the felt, thus leaving 15-55% of the flow area open (Eschmann). The blocking layer is placed near the paper contact side of the felt. The felt can be manufactured by first needling a layer of batt fibers to the base of the felt. The blocking layer is placed on top of this layer of fibers, and then another layer of fibers is placed on the blocking layer. This fiber layer is then needled to the rest of the press felt. This blocking layer essentially creates nozzles for flow within the felt. Water leaving the paper web is accelerated through the open area in the blocking layer. After leaving the pressing gap, the blocking layer retards the flow of water back into the paper web, thus minimizing rewet.

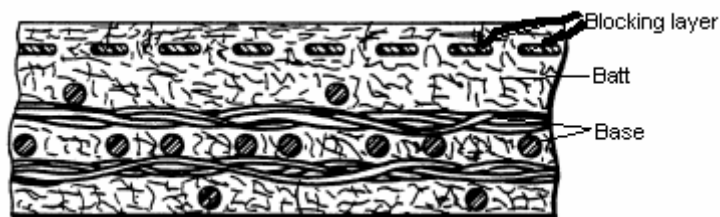


Figure 2.7: Representation of Patent 5,204,171 (Eschmann)

In patent 5,232,768, a barrier layer is placed in the press fabric. The barrier layer has high flow resistance in the thickness direction (z-direction). The barrier layer can be composed of batt fibers extending in the direction of motion of the press felt (shown by the arrow in Figure 2.8 below). These fibers are closely packed to allow high capillary forces to act when the press felt begins expansion. Coupled with the high flow resistance of the barrier layer, these capillary forces prevent water from flowing back to the paper web to a significant extent because the barrier layer retains this water. The barrier layer may also consist of a perforated film with minute holes. This embodiment is shown in Figure 2.8.

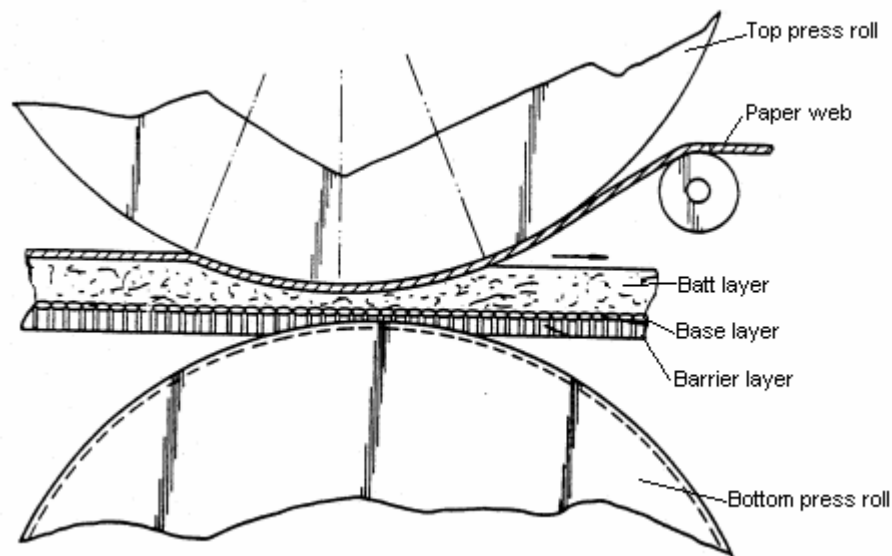


Figure 2.8: Representation of Patent 5,232,768 (Eklund et al.)

Patent 4,988,409 in Figure 2.9 is a three-layered press felt. The top layer is composed of batt with low air permeability. The second layer is a base fabric with substantially higher air permeability than the other two layers. The third layer has the

lowest permeability of the three layers (could be polyurethane or a very compact batt material). When the felt exits the press nip, the bottom layer, due to the low air permeability, remains compressed. The top layer expands at a greater rate. The bottom layer essentially creates a vacuum within the felt, and this vacuum attracts water from the upper layers of the felt. Contact between water in the paper web and water in the surface of the press felt is broken. Thus, capillary forces which cause rewet in conventional felts cannot act in the felt of the proposed invention, and rewet is reduced.

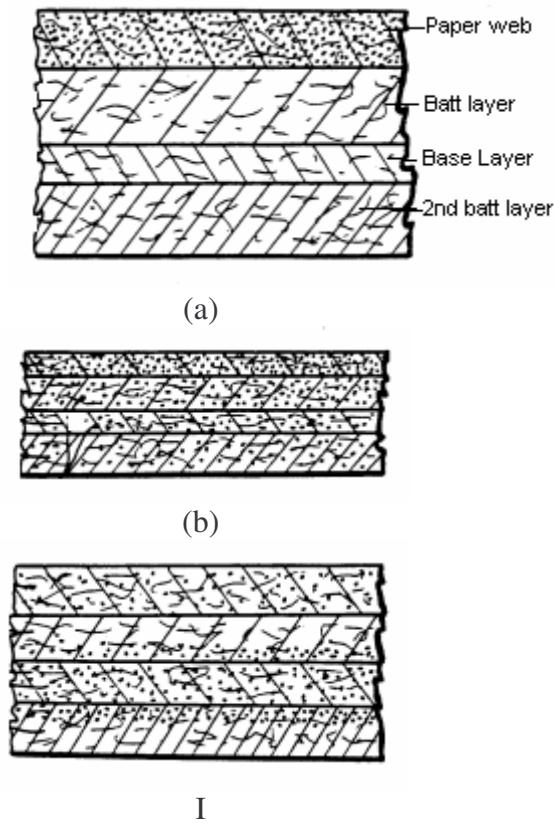


Figure 2.9: Representation of Patent 4,988,409 – (a) Initial State of Web and Felt Prior to Nip (b) Compressed State of Web and Felt, (c) Expanded State of Web and Felt (Nyberg)

In patent 4,199,401 (depicted in Figure 2.10), batt stratification is used to minimize rewet. A layer of coarse batt is placed on top of a layer of fine batt. The denier of the fibers in the fine layer of batt is less than the denier of the fibers in the coarse layer of batt. The higher capillary forces in the fine batt material cause water to remain in the fine batt layer instead of flowing back into paper web.

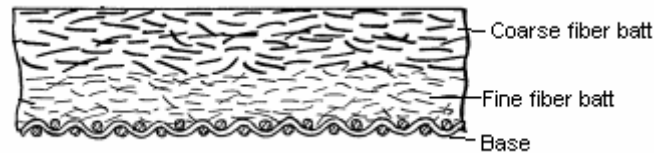


Figure 2.10: Representation of Patent 4,199,401 (Liu and Cottigny)

None of the patents are believed to have had commercial success in the prevention of rewet. It is important to note that none of the above patents attempt to incorporate a three-dimensional valve structure in the press felt as does the proposed design.

2.3 Computer Modeling of Smart Felt

A computer model developed in an AMRC project (Fundamental Model of Wet Pressing) was used to predict the behavior of the smart felt concept. In order to model the smart felt, the permeability and compressibility of the layer was approximated. An iterative process was used to calculate the permeability by combining Darcy's Equation (Equation 1.3) and an equation to approximate the pressure drop across a check valve (Equation 1.4). The compressibility of the smart felt layer was found using the following equation (Rudman 8-24-04):

$$E(P_s) = P_s^{(1-N)} \frac{(c_o + MP_s^N)^2}{c_o MN} \quad (2.1)$$

In Equation 2.1, c_o is the ingoing apparent density of the smart felt, and P_s is the structural pressure. Using the value of E of the smart felt material for at least two different values of P_s ; M and N , which are empirical experimental parameters, can be found. The compressibility, c , is then found using Equation 2.2 (Rudman 8-24-04).

$$c = c_o + MP_s^N \quad (2.2)$$

The smart felt was simulated using both a one-dimensional model and two-dimensional model. The 1-D model is capable of predicting water removal from the sheet based on the effects of felt parameters. The sheet-felt system was simulated as a two-zone and three-zone domain. In the two-zone simulation, the sheet-felt system consists of the sheet and the smart felt. In the three-zone simulation, the sheet-felt system consists of the sheet, a layer of sheet side batt, and the smart felt.

The 2-D spatial model is capable of accounting for in-plane non-uniformities, such as a rough felt, grooved rolls, or openings in the smart felt. The 2-D model was used to predict the uniformity of water removal due to the in-plane spacing of the check valves in the smart felt. The 2-D model was also used to model the sheet-felt system as a two and three-zone domain.

Initial calculations for the 1-D, two-domain sheet-felt system were conducted for an 80 gsm sheet with ingoing solids of 33%. The maximum applied pressure used was 4

Mpa (580 psi). The nip time was varied between 1 and 10 ms. A Young's modulus of 2455 Mpa was used for the smart felt (Rudman 8-24-04). This is the Young's modulus of the Renshape SL 7510, the material used to manufacture a prototype by the Rapid Prototyping Department at the Georgia Institute of Technology. This material, however, was not used in experimentation because of its brittle nature upon completion of the rapid prototyping procedure. The material used in experimentation, Acetron GP, has a similar Young's modulus of 2758 Mpa.

The figure below shows the effect of the smart felt on the outgoing solids of the paper sheet.

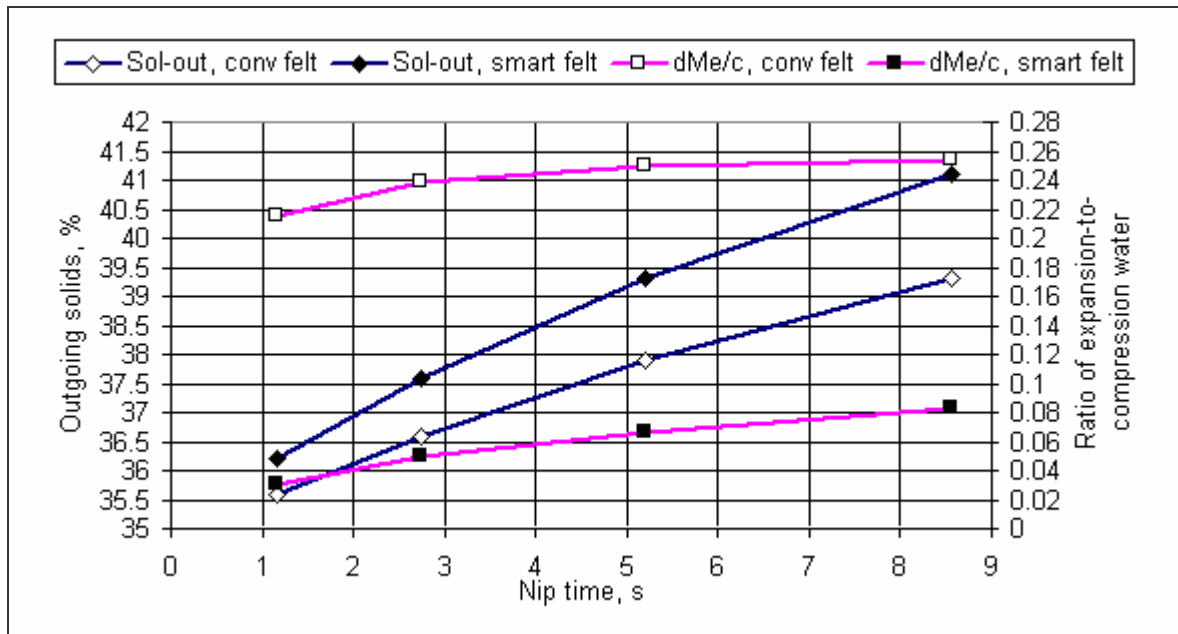


Figure 2.11: Outgoing Solids and Ratio of Expansion-to-Compression Water vs. Nip Time (Rudman 8-24-04)

As can be seen from the figure, the ratio of water removed in compression to the water returned in expansion is much less for the smart felt than for the conventional felt,

resulting in higher outgoing sheet solids for the smart felt. The back flow of water ranged from 3 to 8% for the smart felt and from 22 to 26% for a conventional felt (Rudman 8-24-04).

The effect of smart felt permeability in the expansion phase of wet pressing was simulated and these results are shown in Figure 2.12. As the permeability of the smart felt layer increases on the expansion side of the nip, the outgoing solids of the sheet decreases because of the increasing amount of rewet. The water removed by smart and conventional felt designs is equal for large values of permeability.

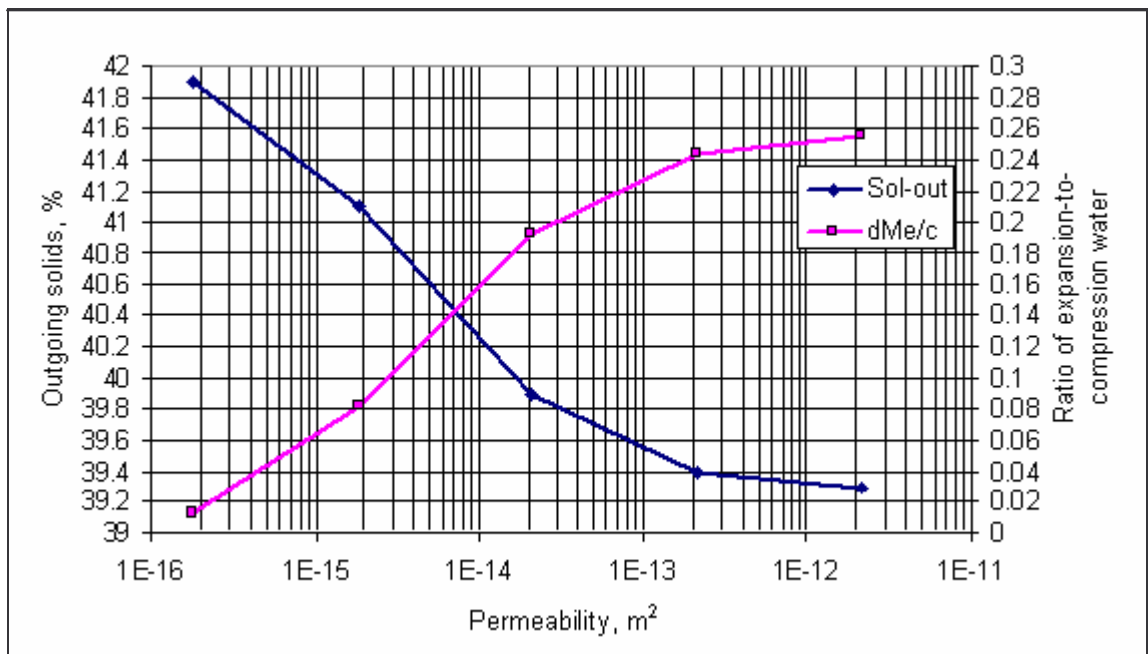


Figure 2.12: Outgoing Solids and Ratio of Expansion-to-Compression Water vs. Permeability of Smart Felt (Rudman 8-24-04)

The water velocity at the sheet-felt interface and the felt permeability are shown in Figure 2.13 for a conventional and smart felt for a nip duration of 9 ms. The permeability of a conventional felt remains relatively constant over the nip, while the

permeability of the smart felt is shown to drastically decrease on the expansion side of the nip. This property is what allows the smart felt to prevent sheet rewetting. The water velocity is shown to be higher in the negative z-direction (towards the sheet) for a conventional felt than for the smart felt.

In Figures 2.14 and 2.15, a three-zone domain is simulated in the sheet felt system. The calculations for these two figures were performed using a nip duration of 9 ms. Figure 2.14 depicts the effect of the sheet side batt basis weight on water removal performance, while Figure 2.15 illustrates the effect of sheet side batt permeability on felt performance.

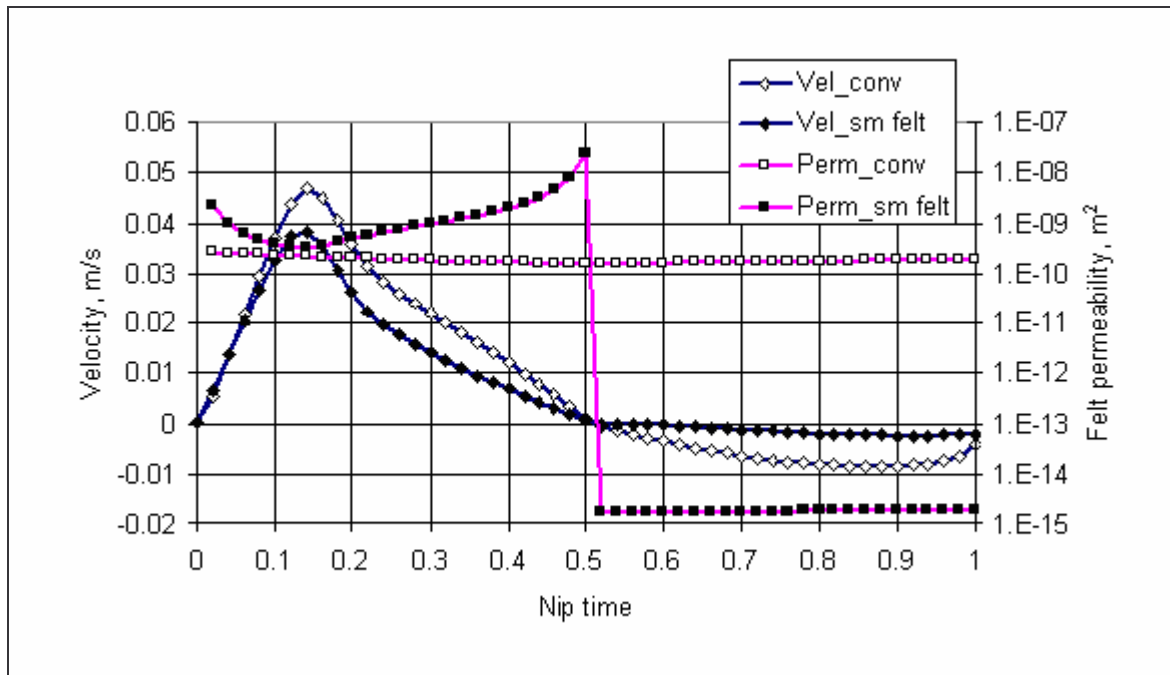


Figure 2.13: Water Velocity at Sheet/Felt Interface and Felt Permeability vs. Nip Time (Rudman 8-24-04)

The ingoing batt permeability for Figure 2.14 was set at $8.25 \times 10^{-12} \text{ m}^2$ (Rudman 8-24-04). The basis weight therefore corresponds to the thickness of the sheet-side batt layer. The simulation shows that as the basis weight of the batt increases (i.e. the smart felt layer is placed further away from the sheet-felt interface), the outgoing solids increases. This seems to contradict accepted rewet theory, which maintains that rewet is a surface effect. Water in the vicinity of the sheet-felt interface is proposed as the primary cause of rewet. In this case, the smart felt layer should be placed as close to the sheet-felt interface as possible so that contact between water in the interfacial region is broken, and water cannot return to the sheet. The results of Figure 2.14 predict the opposite due to the increased hydraulic resistance to water flow for higher weight batt. The higher weight batt, in other words, provides a tighter capillary structure.

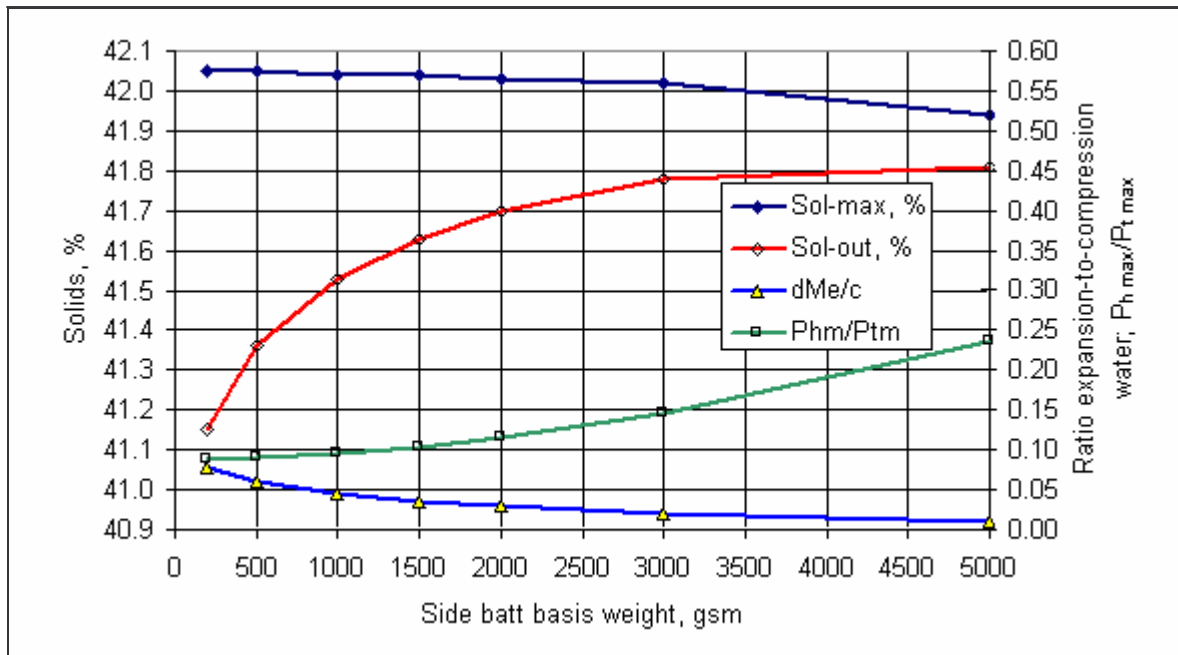


Figure 2.14: Outgoing Solids, Ratio of Expansion-to-Compression Water, and Hydraulic Pressure vs. Sheet-Side Batt Basis Weight (Rudman 8-24-04)

In Figure 2.15, a 500-gsm batt was used in the computations (Rudman 8-24-04). As the permeability of the batt layer decreases, the outgoing solids also decreases as long as the ratio of hydraulic pressure to total pressure is greater than about 0.15. Otherwise, batt permeability has relatively little effect on outgoing solids. This result contradicts the results depicted in Figure 2.14, which show that as hydraulic resistance of the batt increases, the outgoing solids increases. The effects of location of the smart felt layer within the felt and sheet-side batt permeability require further investigation.

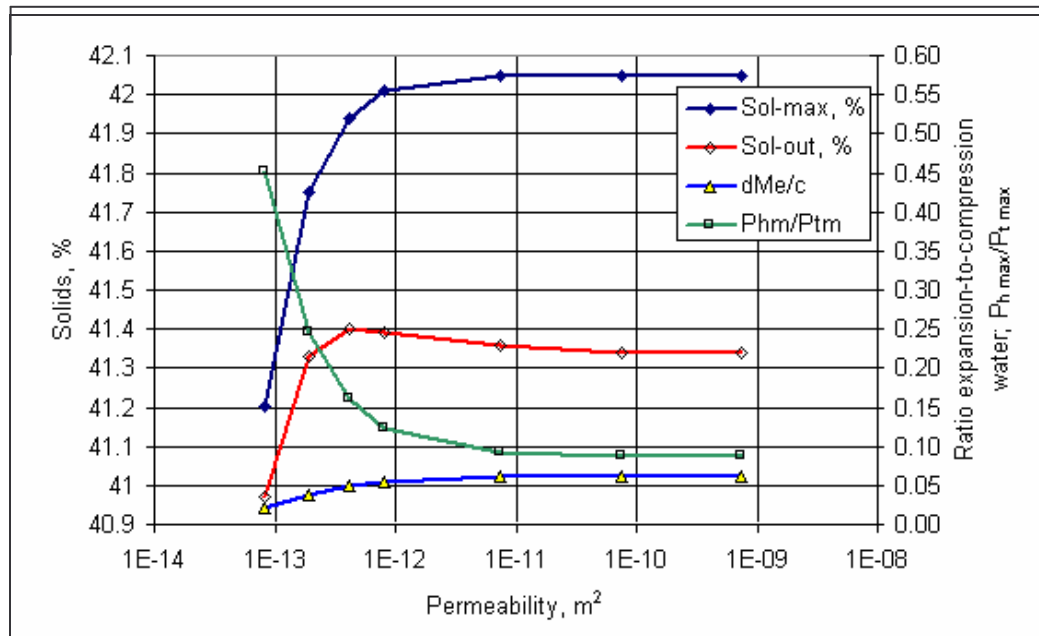


Figure 2.15: Outgoing Solids, Ratio of Expansion-to-Compression Water, and Hydraulic Pressure vs. Sheet-Side Batt Permeability (Rudman 8-24-04)

In the smart felt layer, the spacing of the valves and the opening and closing action of the valves may create non-uniform water removal from the sheet resulting in sheet marking. The domain of the 2-D, two-zone simulation is shown below. In Figure 2.16, m represents the non-dimensional transversal mass coordinate that varies from 0 to 1

with $m=0$ representing the sheet-roll interface and $m=1$ representing the felt-roll interface. The radial coordinate r varies from 0 to R , where R is the total radius of the valve (valve opening plus space between valves) and R_h is the radius of the valve opening.

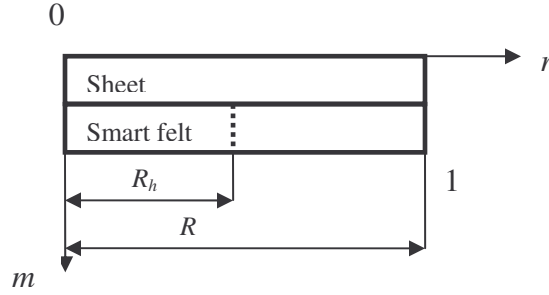


Figure 2.16: Domain of 2-D, 2-Zone Smart Felt Simulation (Rudman 8-24-04)

The boundary conditions are given below. The simulation shown in Figure 2.17 used a maximum pressure of 580 psi and a nip duration of 9 ms (Rudman 8-24-04).

- $P_h(1, r, t) = 0$ for $0 < r \leq R_h$
- $\frac{\partial P_h}{\partial m}(1, r, t) = 0$ for $R_h < r \leq R$

In Figure 2.17, the hydraulic pressure is shown to be high for small valve openings. This ratio decreases as the valve opening increases, effectively increasing the permeability of the valve layer. The outgoing solids increase as the valve opening increases to a ratio of about 0.65. The outgoing solids then slightly decrease resulting from an increase in water backflow. Non-uniformity of pressure application was not

taken into account in this simulation. A larger ratio of R_h/R will likely increase non-uniformity of pressure distribution resulting in non-uniformity of water removal.

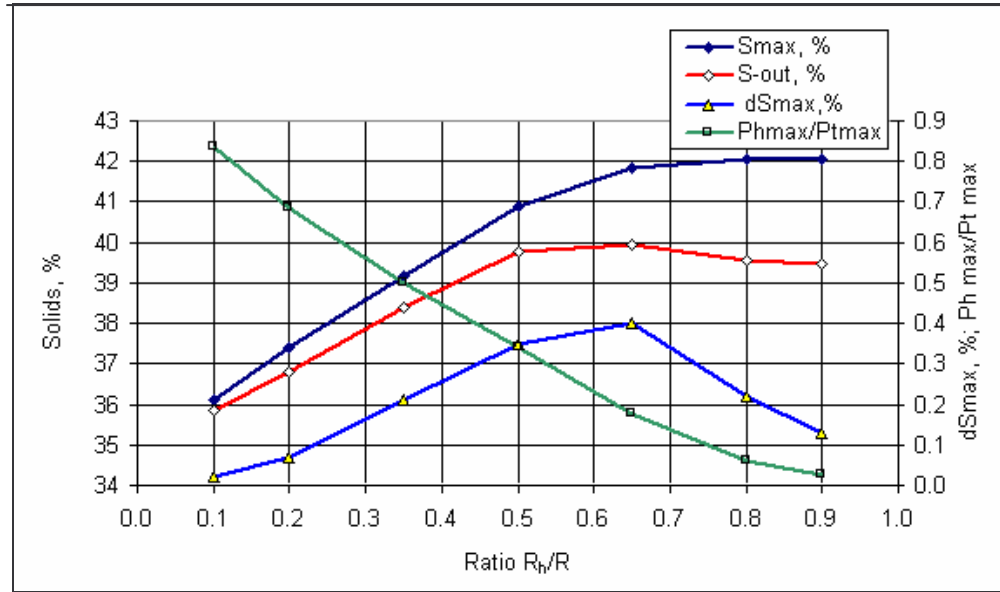


Figure 2.17: Outgoing Solids and Hydraulic Pressure vs. Valve Opening (Rudman 8-24-04)

Figure 2.18 shows a simulation of the smart felt that accounts for varying thicknesses of sheet-side batt. The batt basis weights investigated were 0.5, 1, and 1.5 kg/m^2 (Rudman 8-24-04). The outgoing solids are shown to be higher for thicker batt at small valve openings. Also, as expected, uniformity of water removal increases as the thickness of the batt layer increases.

The results presented in this section indicate, at least theoretically, that the concept of a smart felt is feasible. The smart felt is shown to decrease in permeability on the expansion side of the nip, resulting in reduced rewet of the paper sheet. Applying a layer of sheet side batt is shown to increase the uniformity of water removal without

providing increased back flow of water. The results, however, require further validation through experimental testing.

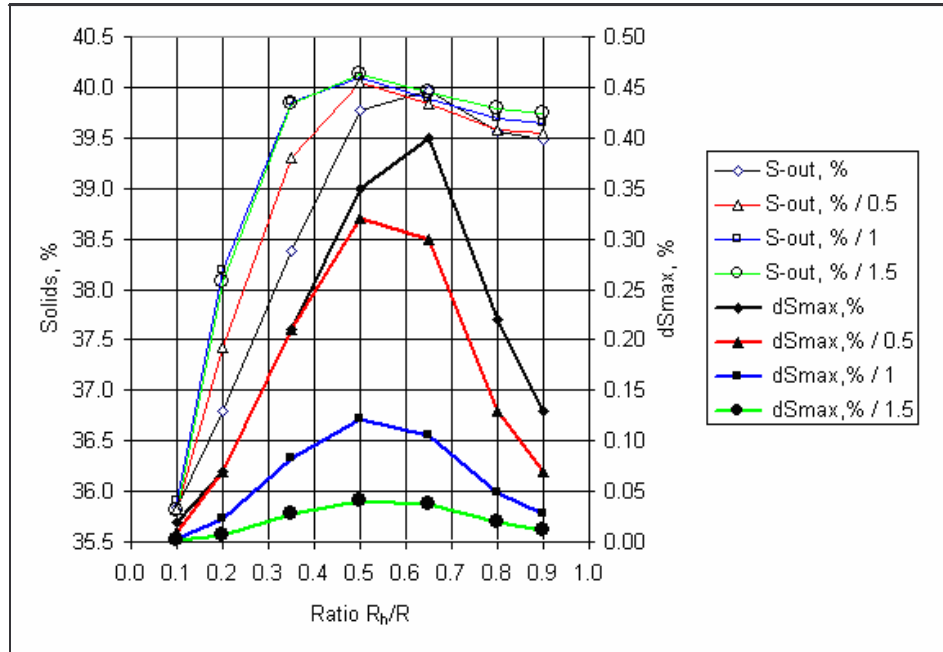


Figure 2.18: Outgoing Solids and Non-uniformity of Water Removal vs. Valve Opening for Various Basis Sheet-Side Batt Basis Weights (Rudman 8-24-04)

CHAPTER 3

METHODOLOGY

3.1 Design of Smart Water Receiver Prototype

In order to experimentally test the feasibility of the smart water receiver concept, flow conditions in a press nip required simulation. A check valve prototype required testing under these flow conditions to predict the behavior of a smart water receiver in a similar environment. A piping system in which a check valve prototype could be tested was designed in order to simulate the flow environment of a wet press nip.

The first step in this process was the design of a check valve prototype. In order to size the prototype, the size of a smart water receiver that could be placed within a conventional press felt was considered. The cantilever beam, which acts as the check valve, for a similar micro-check valve used for micro-fluidic systems has the dimensions given in Table 3.1. Large-scale production of valves of this size, however, is currently not possible due to costs and limitations of the manufacturing process. As can be seen by simplifying Equation 1.2, the angle of deflection of a cantilever beam for a given load is the same for equal length to thickness ratios of the beam. Thus, the same deflection angle can be achieved under a given load by equally scaling the length and thickness of the cantilever beam. Possible dimensions for the cantilever beam for use in a smart valve layer are given in Table 3.2. The size ratio of this beam to the beam in Table 3.1 is 10:1. To test the behavior of a valve of the dimensions given above in either Table 3.1 or Table

3.2 under the flow conditions in a press felt would be extremely difficult due to size limitations.

Table 3.1: Cantilever Dimensions for Valves Used in Micro-Fluidic Systems

Cantilever Dimensions	
Length	600 μm
Width	300 μm
Thickness	10 μm

Table 3.2: Cantilever Beam Dimensions for Valves in Smart Valve Layer

Cantilever Beam Dimensions for the Smart Valve Layer	
Length	6 mm
Width	3 mm
Thickness	0.1 mm

The geometry of the valve was thus scaled to fit in a 1.5". Schedule 40 PVC pipe (inside diameter of 1.61 in. or 40.9 mm). The dimensions of the cantilever beam for the valve prototype are given in Table 3.3. The length ratio of the prototype to the smart valve layer is 5:1. Due to machining error, the thickness of the cantilever for the completed prototype was actually 0.76 mm (instead of 0.50 mm). The deflection of a cantilever of this length and thickness under a given load would thus be the same as the

deflection of a cantilever of length given in Table 3.2 and thickness of 0.152 mm under the same load.

The material used by Hok, et al., for the micro-check valve was silicon due to its desirable mechanical properties (i.e. Young's modulus, tensile strength, natural vibration frequency, etc.). Due to its expense and availability, however, silicon is not a feasible alternative for the smart valve layer. For the smart valve layer, a lower Young's modulus allows the valve to deflect more under a lower pressure differential. However, the cantilever beam must have adequate strength and stiffness to prevent back flow

Table 3.3: Dimensions of Cantilever Beam for Valve Prototype

Cantilever Beam Dimensions for Valve Prototype	
Length	30 mm
Width	15 mm
Thickness	0.5 mm

under the vacuum created during expansion. The maximum pressure that the beam can withstand under reverse pressure is given by Equation 3.1 (Hok et al 392). To use this

$$P_{\max} = 3.5 \frac{\sigma_{\max} t^2}{a^2} \quad (3.1)$$

equation, the cantilever beam must be approximated as a square plate over a square opening with sides of length a . The maximum vacuum created by the paper web upon

expansion is around 90 kPa (Palokangas 103). The sides of the square hole for the top layer in the smart felt were assumed to be of length 3.5 mm for use in the equation above. This length covers approximately the same area of the cantilever beam as a 5 mm x 2.5 mm rectangular opening, which are the dimensions of the openings in the top layer of the smart valve layer (see Figures 3.2 – 3.4). The thickness of the beam is 0.1 mm. If the felt is assumed to provide no vacuum to counter the vacuum of the paper, the yield strength of the material must be at least 31.5 Mpa. The smart valve layer should thus have the lowest Young's Modulus possible while having a yield strength higher than 63 Mpa (this includes a safety factor of 2) .

Acetron GP Acetal was selected as the material to be used to make the cantilever beam. It was chosen, given input on what was desired of the part, by the machinist (G.M. Tooling General Machine Shop) based on availability and machinability. The mechanical properties are given in Table 3.4 (additional properties can be found in Appendix F). The production of a smart valve layer for use in a conventional press felt may require use of different materials based on issues such as cost, manufacturability, chemical compatibility, fatigue life, etc. These issues have yet to be investigated.

In order to approximate the behavior of a check valve in a smart felt, the flow conditions in the felt require simulation in the experimental piping system. The equation governing the behavior of the check valve is given in Equation 1.4 (repeated from Chapter 1).

$$\frac{\rho}{2}(K_L)V^2 = \Delta P \quad (1.4)$$

Equation 1.4 can be non-dimensionalized by dividing both sides by $\frac{\rho}{2}V^2$. K_L , the loss coefficient, is a function of both Reynolds number and geometry (Munson et al. 481). The flow conditions for the smart valve layer can therefore be simulated by scaling the geometry and Reynolds number of the flow in a wet press.

Table 3.4: Mechanical Properties of Acetron GP Acetal
(<http://www.quadrantepp.matweb.com/SpecificMaterialNew.asp?bassnum=P1SM00&group=General>)

Mechanical Properties	
Specific Gravity	1.41
Tensile Strength	66 Mpa
Tensile Modulus	2758 Mpa
Flexural Strength	83 Mpa
Flexural Modulus	2758 Mpa
Shear Strength	55 Mpa
Compressive Strength	103 Mpa
Compressive Modulus	2758 Mpa

Valves in the smart felt are imagined as having the configuration shown in Figure 3.1. The size ratio for the valve opening and cantilever beam of the prototype to the valve layer was scaled on a 5:1 ratio. In order to achieve similar flow conditions, the Reynolds number and geometry for flow in the felt and for flow in the pipe system must be equal. The geometry of the unit cell that is simulated by a 1.5” PVC pipe can be

found by equating the hydraulic diameter ratios for the unit cell and prototype (these calculations are shown in Appendix G). In other words, the ratio of the hydraulic diameter of the unit cell to the hydraulic diameter of the valve opening in the smart felt is set equal to the ratio of the diameter of the pipe to the hydraulic diameter of the valve opening in the prototype. The Reynolds number is given in Equation 3.2.

$$\text{Re} = \frac{\rho V D_h}{\mu} \quad (3.2)$$

In Equation 3.2, V is the velocity of approaching fluid given in the AMRC computer model, ρ is the density, μ is the dynamic viscosity, and D_h is the hydraulic diameter.

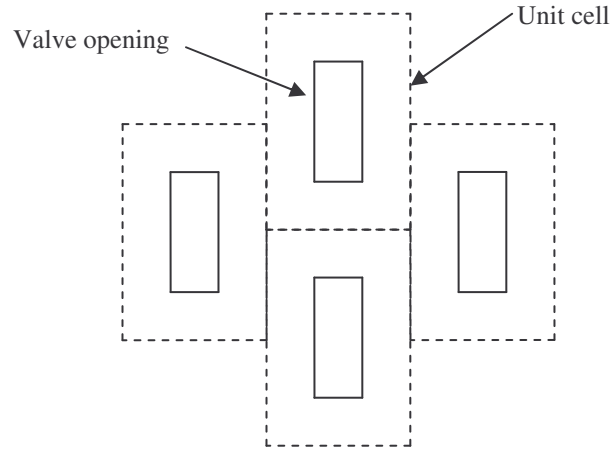


Figure 3.1: Valve Configuration in Smart Felt

D_h is given by Equation 3.3 (Kreith 48). In pipe flow, D_h is simply the pipe diameter.

$$D_h = \frac{4(\text{cross sectional area})}{\text{wetted perimeter}} \quad (3.3)$$

Knowing the hydraulic diameter for the unit cell in the smart valve layer, the Reynolds number through the smart felt can be found. This can then be translated to the Reynolds number for pipe flow for simulation of flow through the smart valve layer. Using a maximum velocity of 0.04 m/s at the sheet felt interface (from Figure 2.13 of computer model), a maximum Reynolds number of near 580.76 is found. Translating this Reynolds number to flow in a pipe gives a maximum flow rate of approximately 1100 ml/min. The flow in the pipe thus needed to be varied between 0 and 1100 ml/min in order to predict the behavior of the smart valve layer for a valve of the size given in Table 3.2 and the spacing given by the hydraulic diameter for the unit cell shown in Figure 3.1..

Another factor considered in the design of the valve layer was the batt layer placed above and below the valves. For the valve to open properly, batt cannot be needed directly to the valve. The valve must contain free space that allows the cantilever to move back and forth and regulate flow. For the valve prototype, the cantilever beam was placed inside a rectangular opening with width and length dimensions slightly more than the width and length dimensions of the cantilever. The height of this opening was 5 mm, which was arbitrarily chosen. In order to size the height of this opening, the in-plane spacing of the valves, the force applied to the valve layer in the press, and the amount of deflection of the cantilever must be considered. Measuring the angle of deflection of the cantilever was addressed during experimentation on the valve prototype to determine the amount of open space needed for the cantilever to move freely under

applicable flow rates. In order to measure the angle of deflection of the cantilever, pins were placed in the rear of prototype as shown in Figure 3.4. Three pins were inserted at a distance of 4.10 mm from the bottom of the cantilever. Pin 1 was inserted at a distance of 28.88 mm from the attached end of the cantilever, resulting in a maximum deflection angle of 8.11° . Pin 2 was located a distance of 25.4 mm from the attached end of the cantilever, resulting in a maximum angle of deflection of 9.26° . Pin 3 was inserted at a distance of 22.45 mm from the attached end of the cantilever, resulting in a maximum angle of deflection of 10.26° . The angle of deflection was measured by comparing the pressure drop at certain flow rates with no pins in place to the pressure drop with each individual pin inserted. The flow rate at which the pressure drop first deviated from the results with no pins in place was noted, and this pressure drop was associated with the angle of deflection corresponding to the pin used in the experiment.

The design drawings and photographs of the valve prototype are shown on the following pages. Dimensioned drawings can be found in Appendix D.

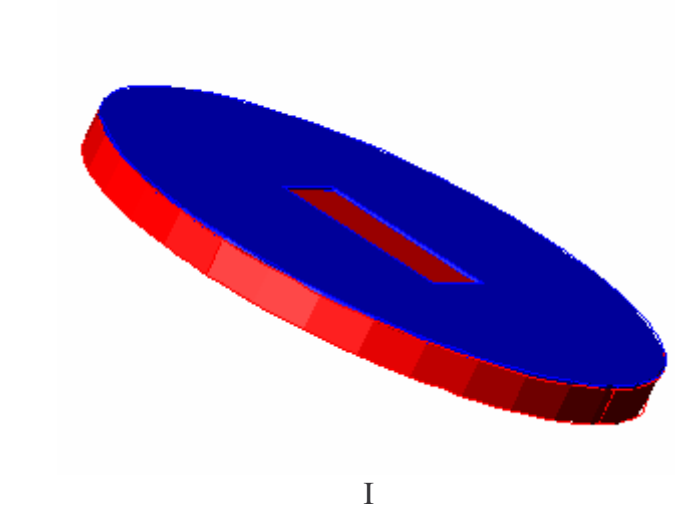
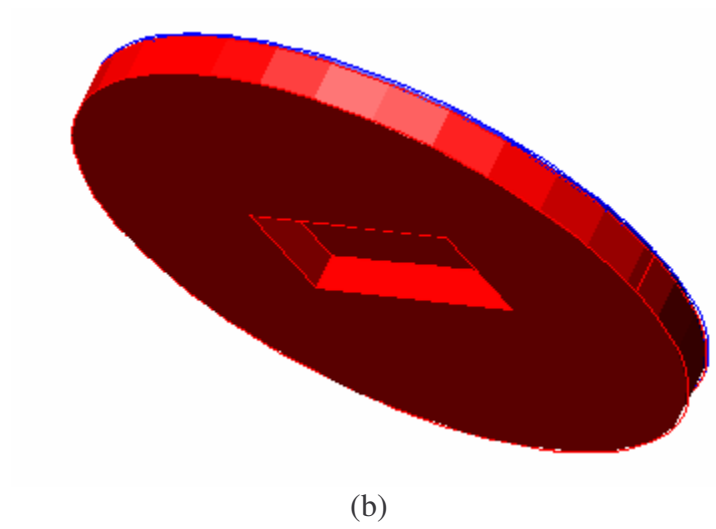
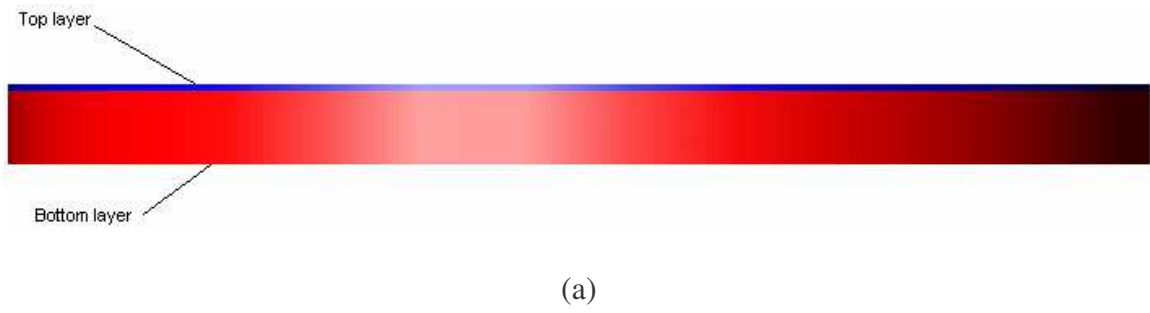


Figure 3.2: (a) Solid Side View of Valve Prototype, (b) Solid Bottom Isometric View, (c) Solid Top Isometric View

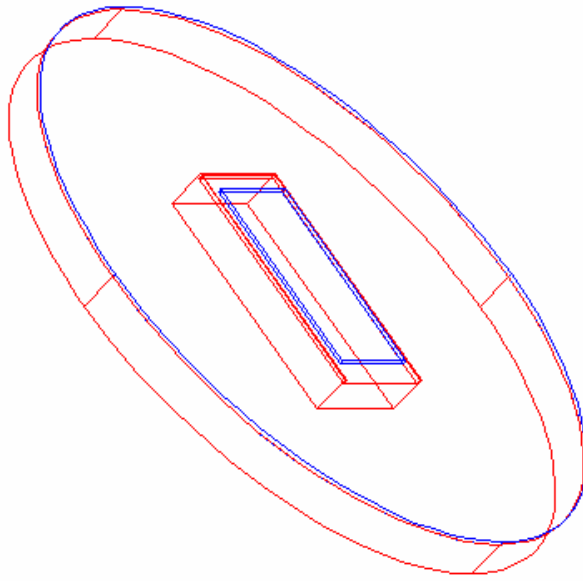


Figure 3.3: 3-D Wireframe View of Valve Prototype

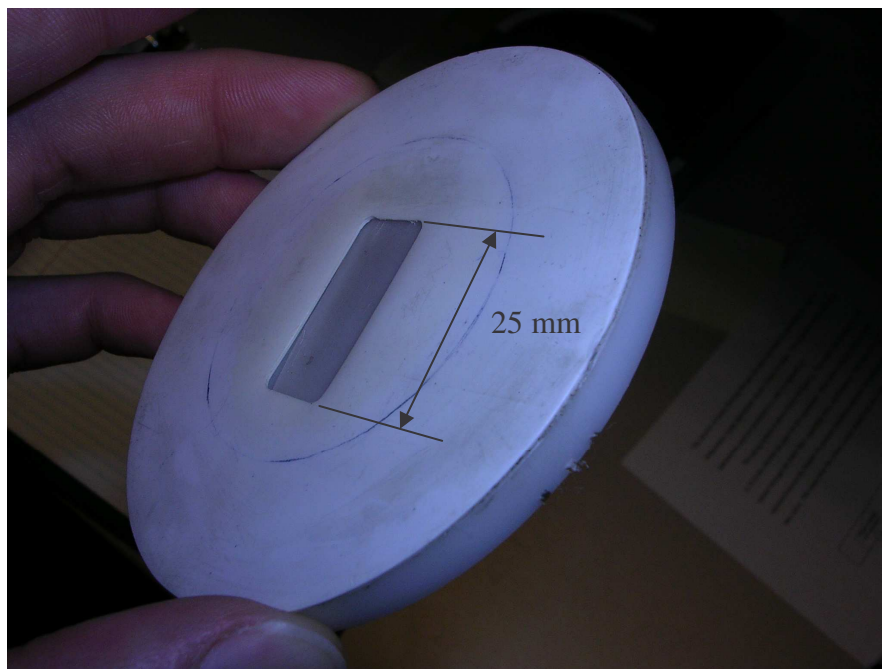


Figure 3.4: Valve Prototype

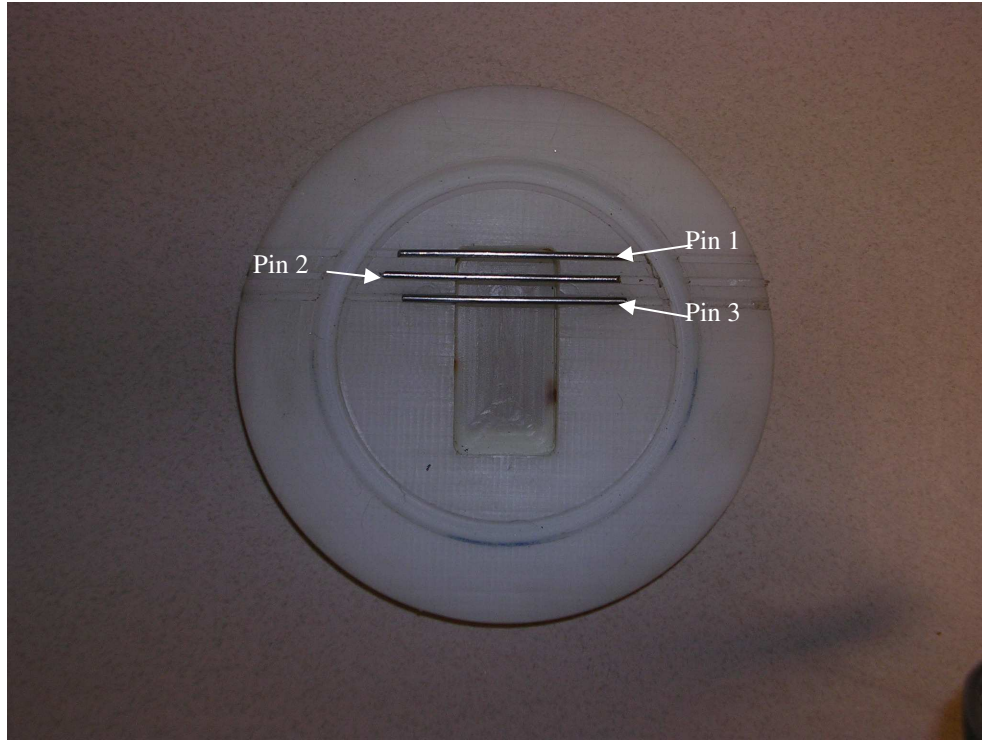


Figure 3.5: Rear View of Pins Placed in Prototype

3.2 Design of Experimental Apparatus

In order to characterize the smart valve layer according to Equation 1.4, the flow rate and pressure drop across the valve prototype required measuring. In accordance with results found in the above section of Chapter 3, the flow meter needed to measure flow in the range of 0 to 1100 ml/min. In order to predict the appropriate range for the manometer, the pressure drop required to deflect a cantilever beam of dimensions and material used for the valve prototype from 0 to $\frac{\pi}{2}$ radians was calculated using Equation 1.2. To use this equation, the pressure drop times the width of the cantilever beam, ΔPw , was substituted for the force per unit length, W . The results of these calculations for Acetron GP Acetal are shown in Table 3.5.

Table 3.5: ΔP Required to Deflect Cantilever by Angle θ for Acetron GP

θ (radians)	ΔP (in. of H ₂ O)
0	0
$\frac{\pi}{32}$	9.02
$\frac{\pi}{16}$	18.04

The maximum angle of deflection being measured for the cantilever was 10.26° or 0.18 radians. Thus the pressure drop measurement required a manometer with a range of at least 16.5 in. of H₂O. The properties of the measuring instruments used are presented in a table in Appendix E.

The piping system is shown below in Figure 3.4. The system was designed in order to fit in the allotted lab space for the experiment and to allow the flow to become fully developed before reaching the valve prototype (entrance length calculations are shown in Appendix A.2). Water flowed from the in-house water system through the water filter, regulating valve, and flow meter. The valve prototype was inserted between the flanges, and the manometer measured the pressure drop across this valve. The water from the system was then emptied into an in-house drain.

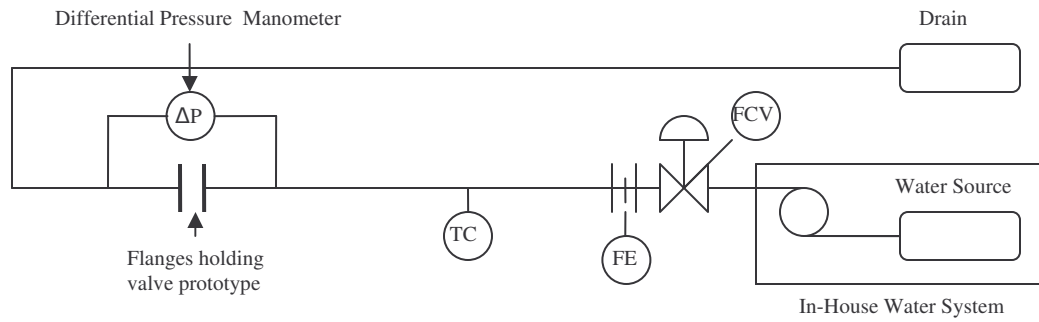


Figure 3.6: Experimental System

The in-house water system in the lab provided adequate head at the appropriate flow rates to test the valve prototype in the piping system. Photographs of the existing experimental set-up are shown below.



Figure 3.7: Experimental System Photograph



Figure 3.8: Flow Meter, Regulating Valve and Water Filter

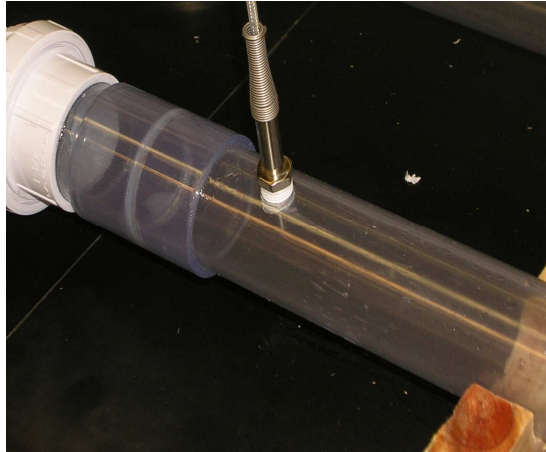


Figure 3.9: Thermocouple

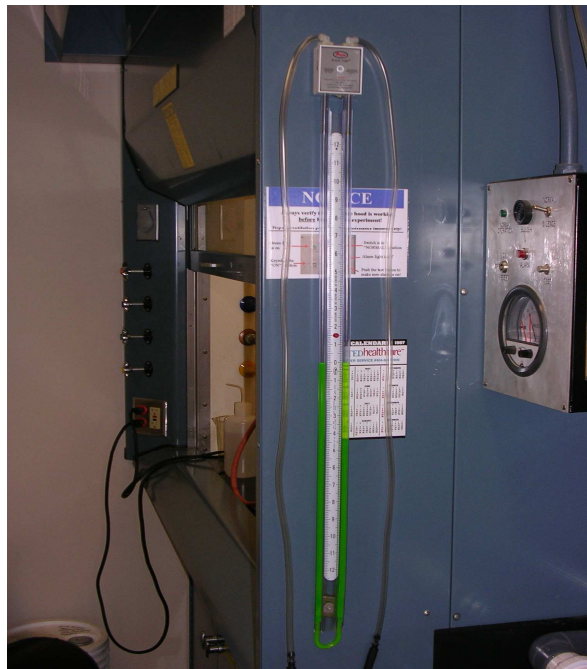


Figure 3.10: Manometer

3.3 Experimental Procedure

Before experiments were run on the valve prototype, the flow meter was calibrated. The flow meter used was a pelton-type turbine flow meter (FLR 1012) from Omega Engineering. This flow meter was outfitted with 3/8" tube compression fittings and required an excitation voltage of 12.5 Vdc. The flow meter gave an output voltage of 0 to 5 V for a working range of 200 to 5000 ml/min.

The flow meter and thermocouple were first connected to the data acquisition system (OMB-DAQ-55 from Omega Engineering), which was wired to a laptop computer. A 500 ml beaker was weighed on a scale. This beaker was used to collect water from the end of the piping system. The water supply was turned on, and care was taken to keep the output voltage below 5 V to avoid damage to the flow meter. The flow was adjusted using the regulating valve and the in-house valves. The flow was adjusted to give an output voltage near one volt. Constant voltages were difficult to achieve because of the fluctuation of the flow rate. Simultaneously, recording of the voltage and temperature data and collection of water from the piping system was begun. Voltage and temperature measurements were taken at a frequency of 19.23 Hz for around one minute. The exact elapsed time of the voltage recordings was measured by the data acquisition system. Recording of the voltage and collecting of water in the beaker were simultaneously concluded. The beaker containing the water was weighed on the scale. The mass flow rate was found by subtracting the weight of the beaker from the total weight of the beaker and water and dividing this by the amount of time of the water collection. The volume flow rate was found using temperature measurements taken by the thermocouple. Using the average temperature of the water found during data

recording, the approximate density of the water was found using property tables for water. The mass flow rate was divided by the density to get the volume flow rate in ml/min. The beaker was emptied, wiped dry and weighed again on the scale. The water flow was then adjusted to give a voltage around two volts. The process described above was then repeated for voltages near two, three, four, and five volts. Once this was done, the average of the voltage readings for each voltage setting was found. The volume flow rates found at tests of approximately one, two, three, four, and five volts were then graphed versus the average of the voltage readings for each voltage setting to generate a calibration curve. This procedure resulted in a similar calibration curve to the one supplied by Omega, thus the experiment was not repeated. The factory calibration was used during experimentation. The results of the flow meter calibration are shown in Figure A.1 in the Appendix A.1.

The valve prototype manufactured from Acetron GP was then inserted into the experimental system. The free end of the cantilever beam was pointing down when inserted. The flange bolts were then tightened to hold the valve in place.

In order to measure the pressure drop across the valve, the following procedure was performed. Pressure loss through the pipe without the valve was considered negligible base on calculations for pressure loss through smooth PVC pipe at the applicable flow rates.

1. The thermocouple and flow meter were connected to the data acquisition system, and the data acquisition system was connected to a laptop computer.

2. The pipe was filled with water. As much air as possible was eliminated from the piping system by allowing air to escape from the tee's to which the manometer would be connected.
3. The manometer was attached to the piping system. The manometer used in this experiment was an slack tube manometer from McMaster Carr. The manometer measured the pressure differential by the mechanical displacement of a column of water and had a range of 0" to 24" of water with a resolution of ± 0.1 " of water.
4. The system was leveled by adjusting the pipe to get a manometer reading of 0".
5. The flow was started and adjusted to a flow rate of 250 ml/min.
6. The pressure drop reading was taken from the manometer.
7. The data acquisition was initiated to record the temperature and flow rate. The flow rate and temperature were then recorded for 100 scans at a scan rate of 1.0549 Hz.
8. The pressure drop from the manometer was recorded after approximately 50 scans of the data acquisition system.
9. Data acquisition was ceased, and the pressure drop was recorded again.
10. The flow was stopped.
11. The manometer was unhooked.

Steps 2-11 were performed 5 times each at flow rates of 250, 500, 750, and 1000, and 1250 ml/min. The results for these experiments are shown in Chapter 4.

Pin 1 was then inserted into the prototype. The deflection of the cantilever beam required to reach pin 1 was measured with a caliper. The distance from the attached end of the cantilever beam to the pin location was then measured. The angle of deflection

was then found by taking the arctangent of the cantilever deflection divided by the distance from the attached end to the pin. The angles of deflection for the other two pin locations were found in the same manner. The prototype was placed between the flanges and the above procedure was performed 5 times each at flow rates of 250, 500, 750, and 1000, and 1250 ml/min. This process was repeated for pin 2 and pin 3.

At the flow rates where the pressure drop deviation was first observed, the intervals were halved (see Figures 4.7, 4.9, and 4.11 in Chapter 4). The pressure drop for pin locations 1 and 2 were measured at 375 and 625 ml/min, while the pressure drop for pin 3 was measured at 1125 ml/min. These tests were performed to more accurately predict the pressure drop associated with the angle of deflection of the cantilever beam. These results are shown in Chapter 4.

CHAPTER 4

RESULTS AND DISCUSSION

Figures 4.1 and 4.2 depict the results of pressure drop experiments performed on the valve prototype for flow rates of 250 ml/min to 1250 ml/min. The flow rate is shown to be a polynomial function of order 2 in terms of the pressure drop across the valve. These figures serve as the basis for comparison for experiments run on the prototype with pins inserted in one of the three locations. These experiments allowed the correlation of the angle of deflection of the cantilever beam with flow rates through and pressure drops across the valve.

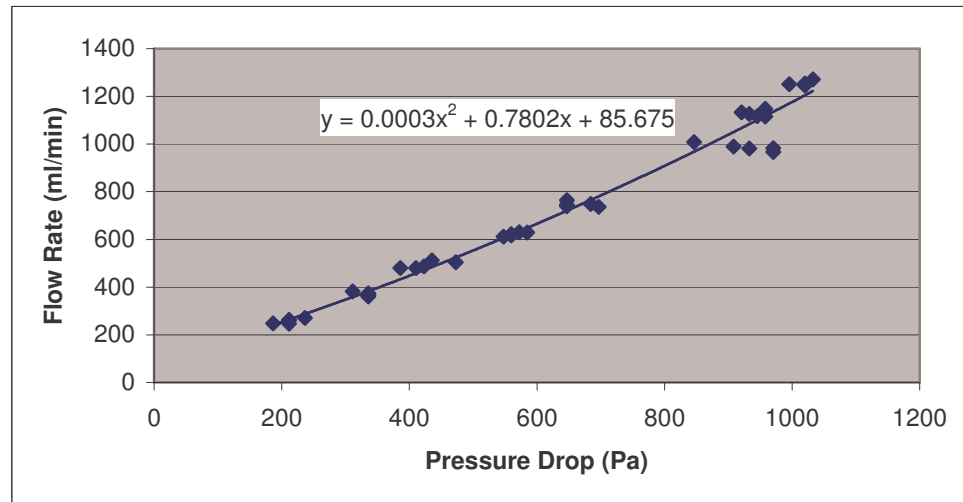


Figure 4.1: Flow Rate vs. Pressure Drop with No Pins in the Prototype

Figure 4.2 shows the loss coefficient versus the Reynolds number. For the calculation of the loss coefficient, the density of water flowing through the pipe was

assumed constant due to the water temperature remaining near room temperature throughout the experimentation. The value used for the density was 997.97 kg/m^3 , which is the density of water at 22°C (Dewitt and Incropera 846). This data is best fit by a power curve given by the equation in the figure.

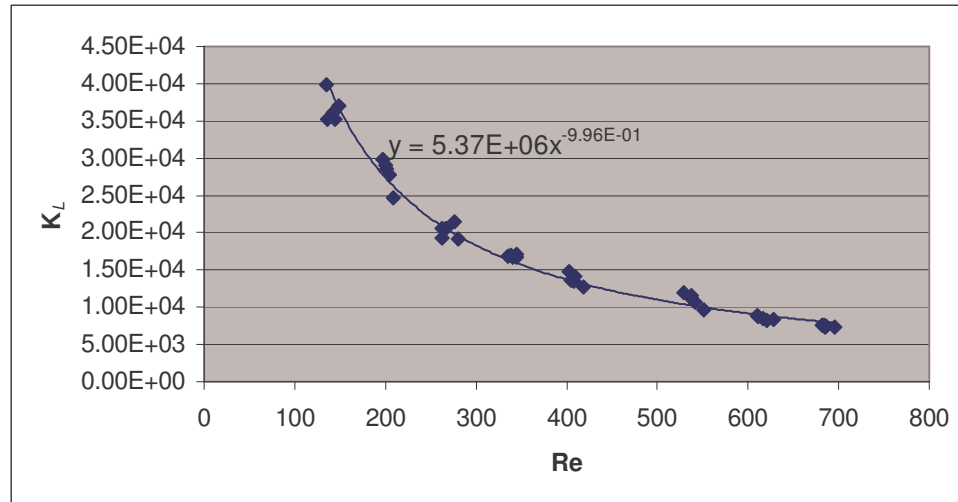


Figure 4.2: Loss Coefficient vs. Reynolds Number with No Pins in the Prototype

The graphs above show that at Reynolds numbers, comparable to Reynolds numbers in the press section of a paper machine, water is able to pass through the valve with very little pressure loss (maximum of 1.03 kPa at 1250 ml/min). According to Szikla, the hydraulic pressure in a press felt can reach up to 0.4 Mpa (163). This pressure is more than adequate to open the valve. Assuming the free space behind the cantilever beam is filled with atmospheric air, the cantilever could potentially be exposed to a pressure differential of approximately 0.3 Mpa. This data seems to indicate that valves of similar mechanical properties placed in a press felt should function properly on the ingoing side of the press nip.

Figure 4.3 compares the pressure loss across the valve with no pins in place to the pressure loss with pin 1 inserted in the prototype. The pressure loss for the test with pin 1 in place is first observed to deviate at 500 ml/min. The average pressure loss at this flow rate without any pins in place was 423 Pa, while the average pressure loss with pin 1 in place was 498 Pa. The location of pin 1 corresponds to an angle of 0.14 radians (8.11°). Therefore, at a pressure drop of 423 Pa and a flow rate of roughly 500 ml/min, the angle of deflection of the cantilever beam is approximately 8.11°.

Figure 4.4 compares the loss coefficients for the valve without any pins in place and with pin 1 in place. The loss coefficient also begins to differ at a Reynolds number corresponding to a flow rate of 500 ml/min. The difference between the two data sets is not as pronounced in this figure as in Figure 4.3 because of the equation used to calculate K_L (Equation 1.4).

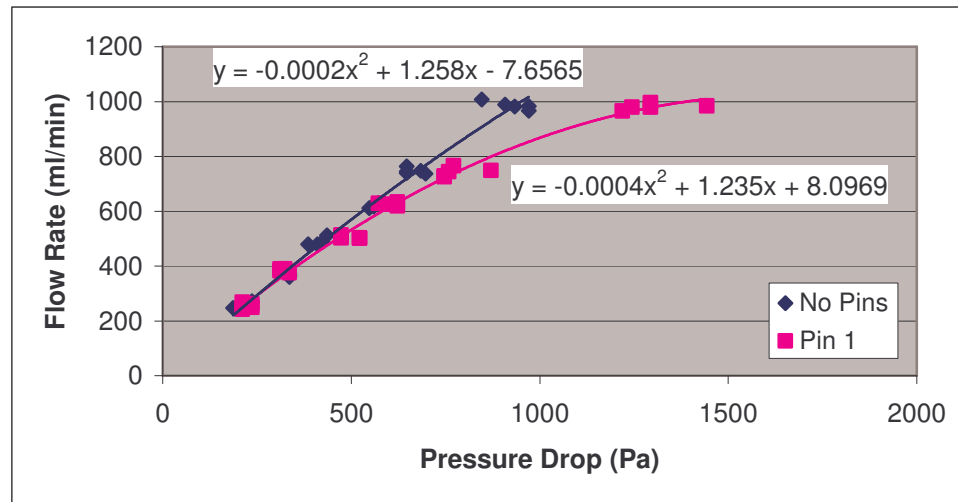


Figure 4.3: Flow Rate vs. Pressure Drop Comparison for Pin 1

For instance, at a flow rate of 500 ml/min, the difference in the pressure loss between the two data sets is 95 Pa. The velocity is on the order of 10^{-3} , and the inverse of this value is squared in the calculation of K_L , rendering the pressure loss difference of 95 Pa almost negligible.

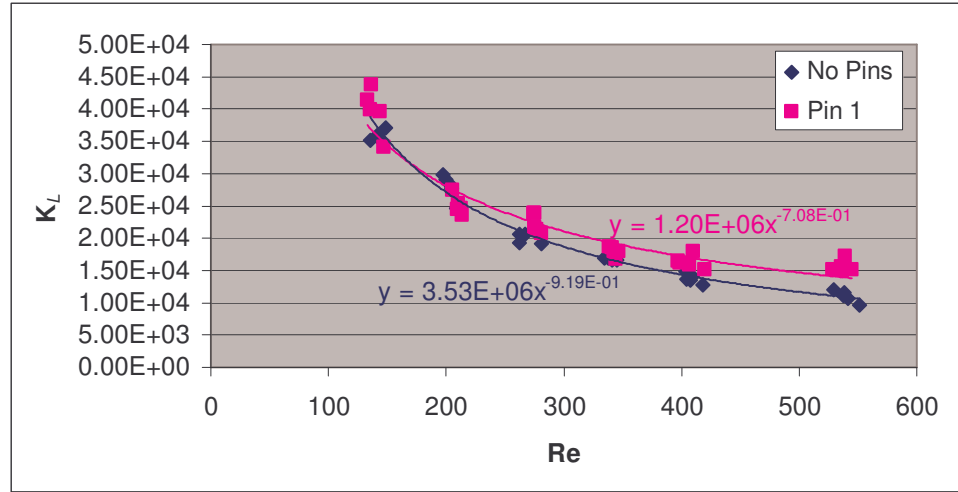


Figure 4.4: Loss Coefficient vs. Reynolds Number Comparison for Pin 1

Figures 4.5 and 4.6 compare the pressure loss across the valve and the loss coefficient of the valve for the experiments conducted with no pins in place and with pin 2 in place. As expected, the pressure loss begins to differ at a higher flow rate than in the experiment with pin 1. The location of pin 2 corresponds to a larger angle of deflection, 0.162 radians (9.26°). The pressure loss begins to digress at a flow rate of approximately 750 ml/min. The average pressure loss at this flow rate with no pins in place is 664.4 Pa. Thus, at a pressure loss of 664.4 Pa, the angle of the deflection of the cantilever is roughly 9.26° .

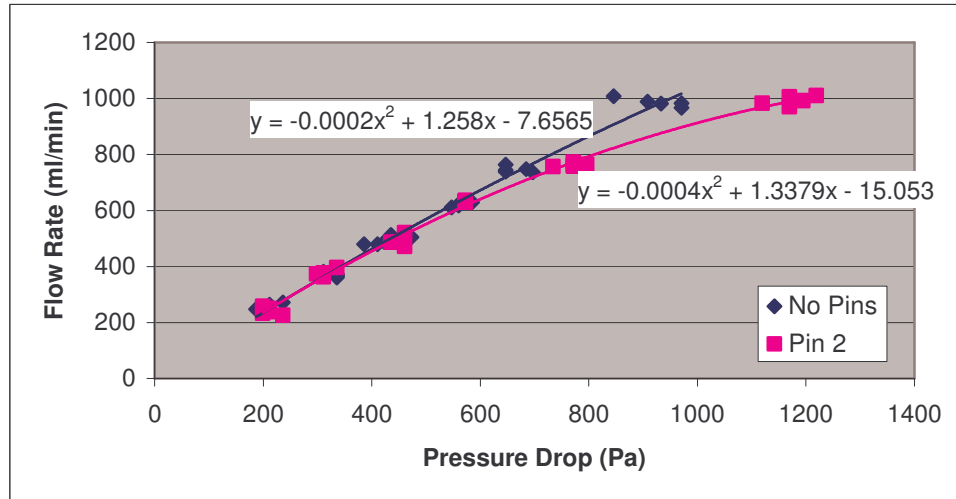


Figure 4.5: Flow Rate vs. Pressure Drop Comparison for Pin 2

Similar to the results of the tests with pin 1, the loss coefficient does not exhibit the deviation from the tests on the prototype with no pins as much as the pressure loss data. The loss coefficients for these two experiments are very similar.

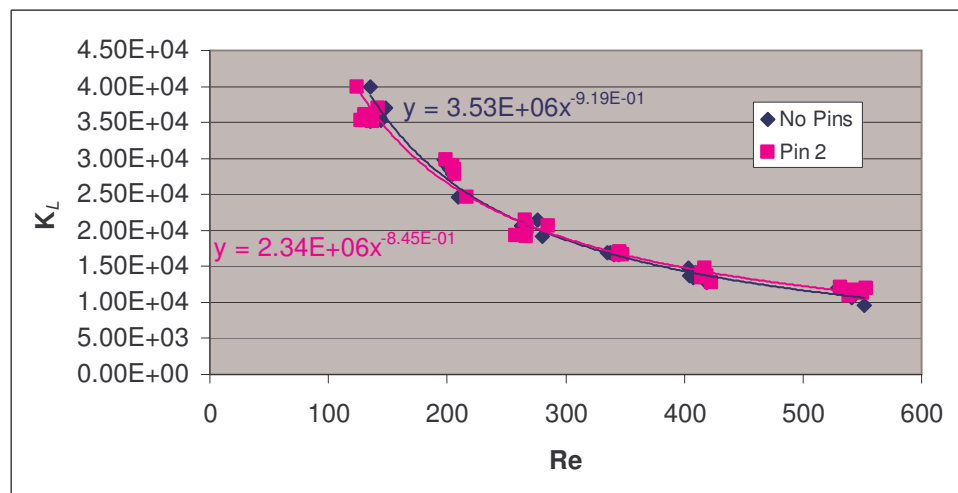


Figure 4.6: Loss Coefficient vs. Reynolds Number Comparison for Pin 2

Figures 4.7 and 4.8 compare the pressure loss and loss coefficient of tests run on the prototype with pin 3 in place with tests having no pins inserted in the prototype. The two data sets remain similar until the flow rate nears 1250 ml/min. At this flow rate, the average pressure loss with pin 3 in place is 1092 Pa, while the average pressure loss with no pins in place is 1018 Pa. The location of pin 3 corresponds to an angle of deflection of the cantilever of 0.179 radians (10.3°). The cantilever thus has an angle of deflection of 10.26° at a flow rate of 1250 ml/min and a pressure drop of 1018 Pa.

Figure 4.8 compares the loss coefficients for pin 3 experiments and experiments with experiments without pins in the prototype. These data sets, as with experiments for pin 1 and pin 2, are very similar.

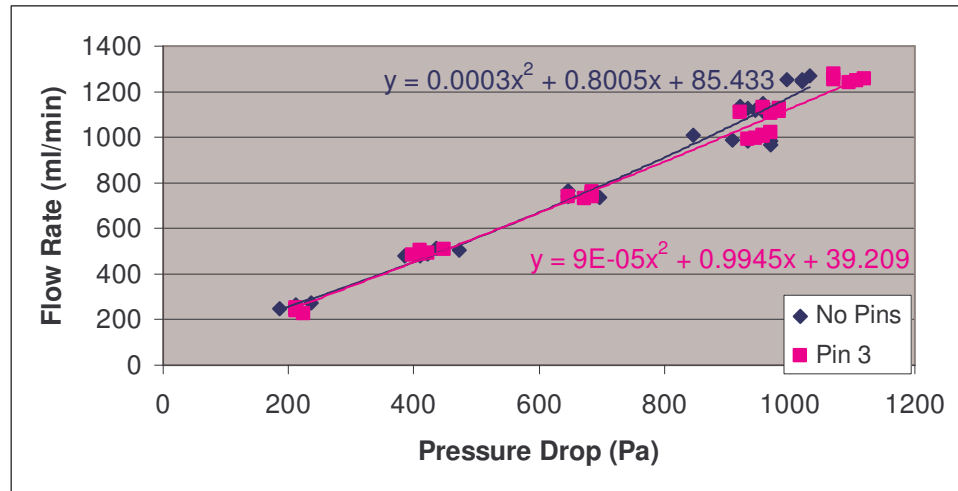


Figure 4.7: Flow Rate vs. Pressure Drop Comparison for Pin 3

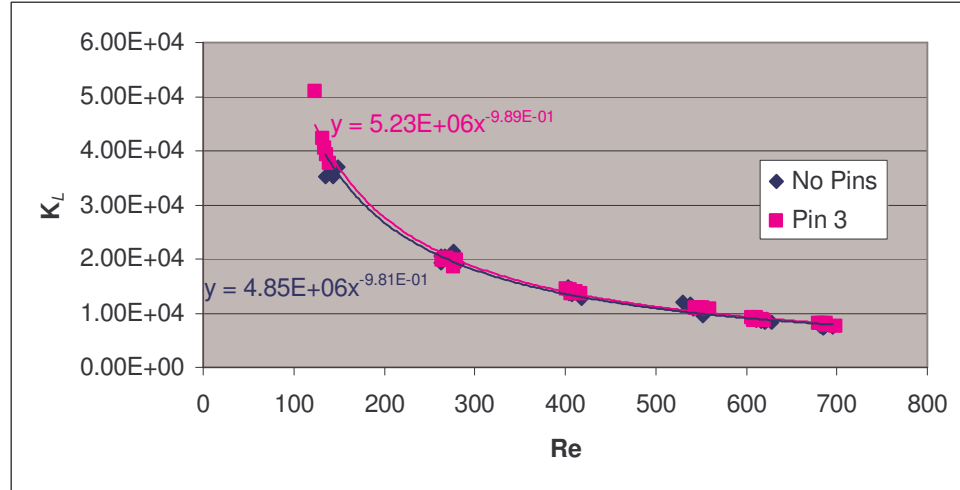


Figure 4.8: Loss Coefficient vs. Reynolds Number Comparison for Pin 3

In Figure 4.9, the angle of deflection of the cantilever is graphed versus the pressure drop across the valve. These data points do not correspond to the values in Table 3.5 calculated from Equation 1.2. The pressure values in the table are much higher than those predicted from experiments run on the prototype. A possible reason for this is the pressure recovery that occurs after flow passes through the valve. To better gauge if the behavior of the cantilever is governed by Equation 1.2, pressure measurements should be taken before pressure recovery occurs (i.e. the pressure tap should be located as close to the exit of the valve as possible).

As can be seen from Figure 4.9, the angle corresponding to a pressure drop of 0 Pa does not correspond to an angle of deflection of 0 radians as would be expected. This is due to inelastic deformation of the cantilever beam. With no flow passing through the valve, the beam was deflected 0.0485 radians.

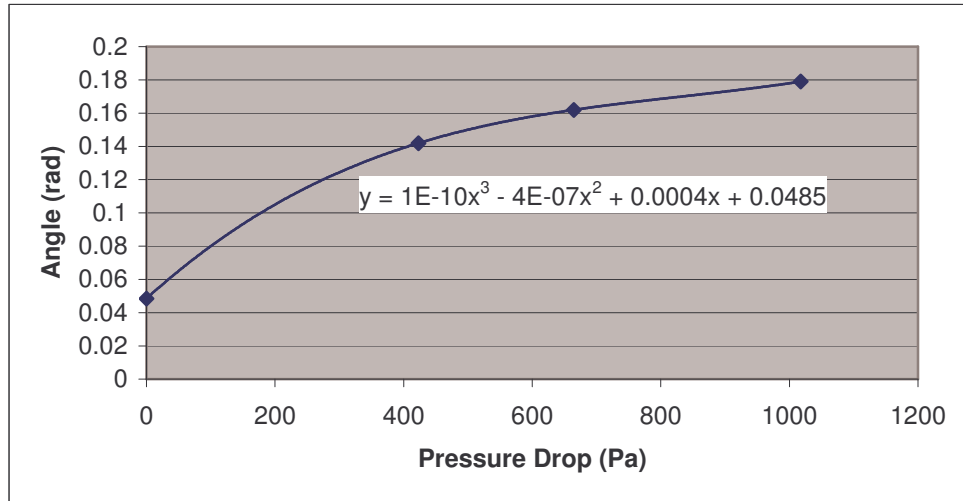


Figure 4.9: Angle vs. Pressure Drop for Cantilever Beam

Figure 4.10 can be generated by plotting the angle of deflection versus the velocity of water approaching the valve.

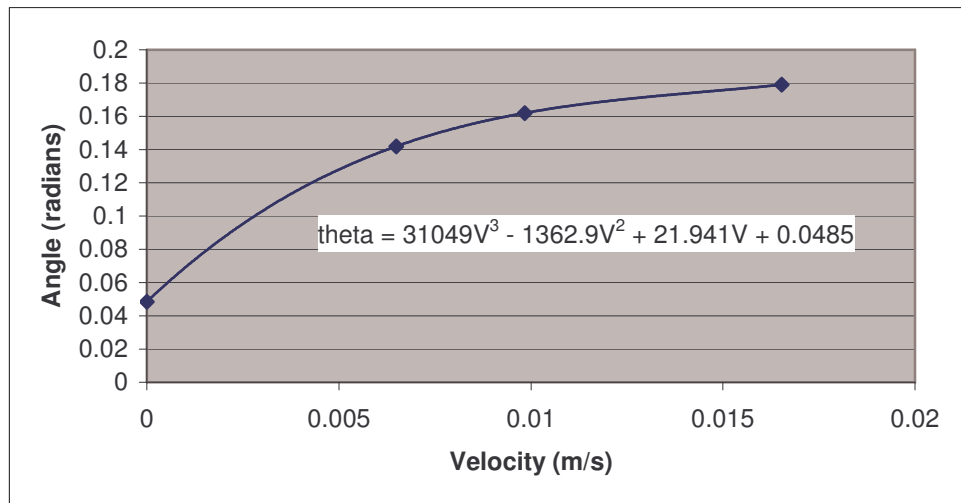


Figure 4.10: Angle vs. Velocity for Cantilever Beam

If the angle of deflection is assumed to be a function of velocity and using 0.0485 radians as the reference, or zero point, the angle of deflection can be predicted for the maximum velocity in the smart valve layer (0.04 m/s) by extrapolating the equation shown in Figure 4.10. The predicted angle for this velocity is 0.68 radians, or 39.2°. The deflection of the free end of the cantilever beam of dimensions given in Table 3.2 at this angle is 4.9 mm (these calculations are shown in Appendix A.3). Based on this extrapolation, the bottom layer of the smart valve layer would thus need to be 4.9 mm thick to allow the beam to freely move back and forth without being restrained by the felt. This would require altering the thickness of a conventional felt to a large degree, which would probably not be economically feasible. This prediction, because extrapolation is required, is uncertain, however. In order to validate this extrapolation, a valve with a cantilever beam of dimensions given in Table 3.2 may require testing.

CHAPTER 5

CONCLUSIONS AND RECOMMENDATIONS FOR FUTURE WORK

A smart water receiver has been proposed for use in the wet press section of a paper machine. The purpose of the smart water receiver is to prevent rewetting of the paper sheet upon exiting the press nip, and thereby save energy in the steam drying section of a paper machine. This rewetting can occur through capillary action, a pressure differential between the paper web and press felt, and film splitting.

The proposed smart water receiver consists of multiple check valves in a thin layer of the press felt. The valves function by the movement of a cantilever beam exposed to a differential pressure. The beam swings open in forward flow and is forced closed under reverse flow (flow from the felt to the paper). The valve therefore inhibits water from returning to the paper web by preventing flow caused by the pressure gradient between the web and felt and by eliminating the capillary action between columns of water on either side of the valve.

The smart water receiver concept was tested both with a computer model and by experiment. The computer model predicted an increase of solids content of the paper sheet of 2.6% by using the smart water receiver as opposed to a conventional press felt. Through experiment, the behavior of the valve layer under flow conditions on the ingoing side of the nip was predicted. This was done by testing a valve prototype of geometry and mechanical properties similar to what might be used in a smart valve layer in a piping system. The results of experimental testing showed that the valve would open under flow

conditions similar to those in a press nip. The experiments also proved that restricting the movement of a cantilever beam under flow and observing the difference in pressure drop caused by this restriction is a viable method of measuring the angle of deflection of the cantilever beam. The angle of deflection for a smaller valve was predicted based on the velocity of water approaching the valve. Using this prediction, the thickness of the felt would need to be altered to a significant degree to allow the cantilever freedom of movement. Altering this thickness dimension may not be feasible. However, because the data from the experiments that were conducted required extrapolation, this prediction remains inconclusive without further testing. An accurate prediction of the angle of deflection may require testing a valve of the same size to be used in the press felt.

Several other issues also remain to be investigated, such as the behavior of the valve in reverse flow, the effect of the valve layer on pressure uniformity, costs of different materials that could be used for the valve layer, cleanability and runnability of the valve layer, shape of the valve seat, and alternate valve designs. The behavior of the valve in reverse flow and the effect of the valve layer on pressure uniformity could be investigated using the MTS press at the Institute of Paper Science and Technology. A sample valve layer, such as the one shown in Figure 5.1, that is the same size as a conventional press felt sample for the MTS press could be tested under loads analogous to those in a press nip to determine if the valve layer prevents rewet upon expansion. The effects of batt layer thickness placed on the valve layer and the effect this has on pressure application to the paper web could also be tested with such an experiment.

Although further testing is required, the smart water receiver concept, according to experiments performed to date, is feasible. If the concept works as predicted,

tremendous savings in energy could be achieved in the paper industry. The further development of such a concept is recommended.

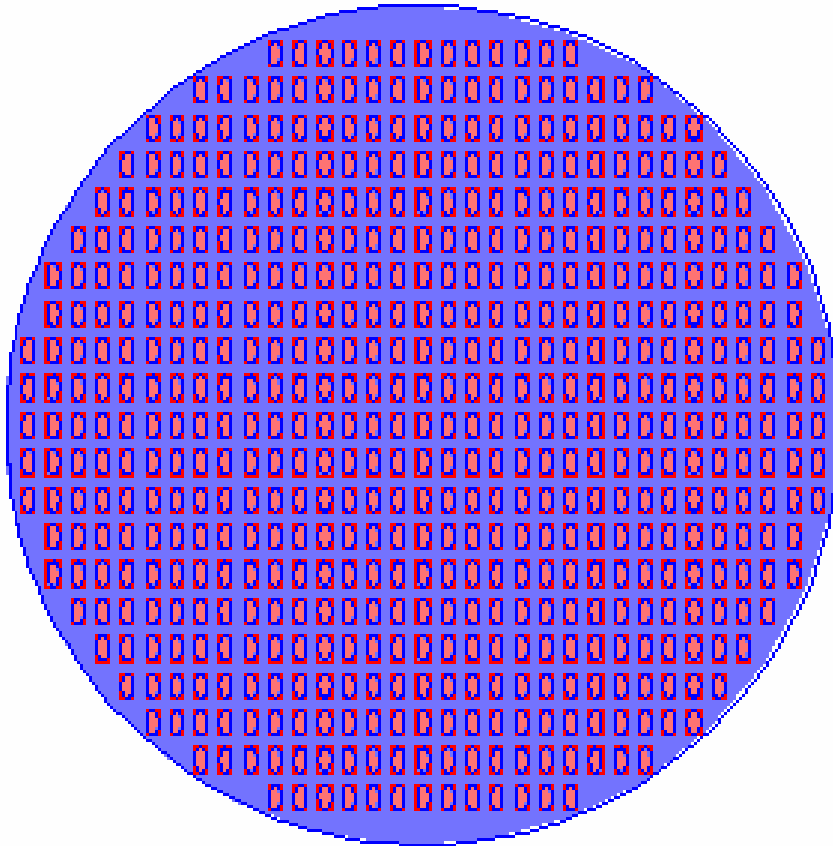


Figure 5.1: Sample Valve Layer for Experimentation in MTS Press

APPENDIX A

RAW DATA

A.1 Calibration Data

Table A.1: Calibration Data for Measured Calibration of FLR 1012

Voltage (Avg.)	Measured Flowrate (mL/min)	Trendline FR	Linearity Error (%)
4.481956214	4974.682823	4850.51891	-2.56%
3.648851963	3818.348079	3924.27361	2.70%
3.040198458	3172.326113	3247.57264	2.32%
1.910406649	1987.812381	1991.47011	0.18%
1.090406646	1140.634567	1079.79410	-5.63%

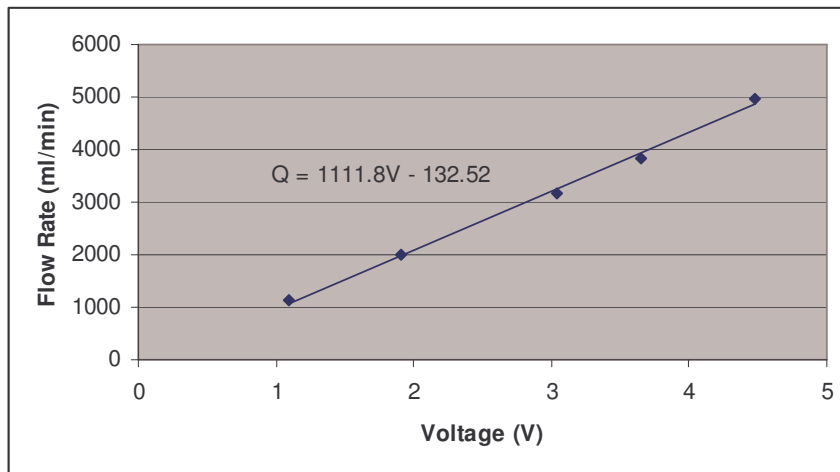


Figure A.1: Calibration Curve for Measured Calibration of FLR 1012

Table A.2: Factory Calibration Data for FLR 1012

Avg. Flowrate (mL/min)	Voltage (avg.)	Trendline FR	Linearity Error (%)
5000	5	4994.287	-0.11%
2500	2.53	2513.666	0.54%
1000	1.02	997.173	-0.28%
500	0.52	495.023	-1.01%

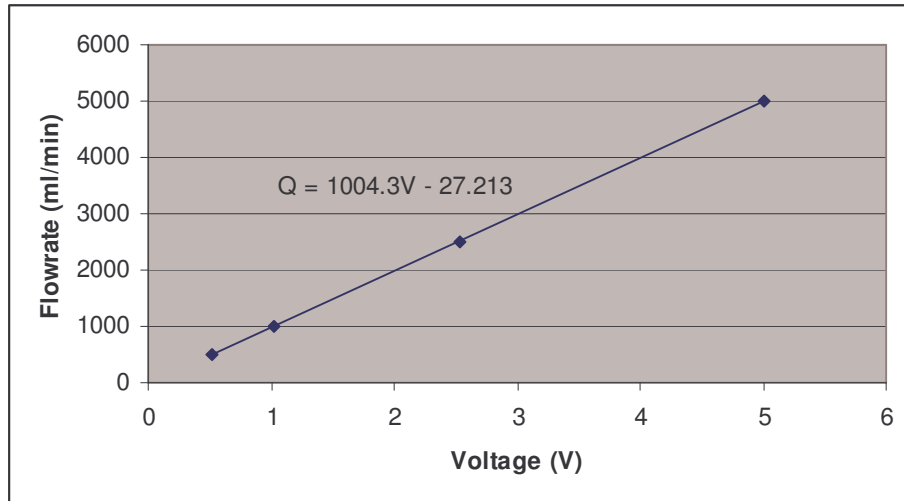


Figure A.2: Factory Calibration Curve for FLR 1012

A.2 Entrance Length Calculations

Table A.3: Constants

density @ 22°C (kg/m ³)	997.97
viscosity (Pa•s)	0.000964042
Flow Diameter (in.)	1.61
Flow Diameter (m)	0.040894
Conversion (in. to m)	0.0254
Flow Area (m ²)	0.001313436
Length conversion (m to ft)	3.2808
Flow rate conversion (ml/min to m ³ /s)	1.67E-08
Pressure conversion (in. of H ₂ O to Pa)	248.84

Table A.4: Entry Length Calculations

Flow rate (ml/min)	Flow rate (m ³ /s)	Velocity (m/s)	Re	Laminar Entry Length (m)	Turbulent Entry Length (m)	Entry Length (ft)
500	8.33E-06	6.34E-03	268.5	0.6701521	-0.470672926	2.1986351
1000	1.67E-05	1.27E-02	537.0	1.3399337	-0.295840725	4.3960545
1250	2.08E-05	1.59E-02	671.3	1.6748591	-0.239557327	5.4948779
1500	2.50E-05	1.90E-02	805.6	2.0097927	-0.193570443	6.5937280
2000	3.33E-05	2.54E-02	1074	2.6796724	-0.121008524	8.7914694
3000	5.00E-05	3.81E-02	1611	4.0194532	-0.018738243	13.187022
4000	6.67E-05	5.08E-02	2148	5.3592449	0.053823677	0.1765847
5000	8.33E-05	6.34E-02	2685	6.6990409	0.110107074	0.3612392

A.3 Extrapolation for Determination of Angle of Deflection

Table A.5: Projection from Figure 4.10 with Intercept at Zero

Calculations		
Velocity (m/s)	Angle (radians)	Angle (degrees)
0.04	0.684136	39.19810541
Formulas		
Velocity (m/s)	Angle (radians)	Angle (degrees)
0.04	$31049 \cdot V^3 - 1362.9 \cdot V^2 + 21.941 \cdot V$	$\theta^* (180/\text{Pi})$

APPENDIX B

EXPERIMENTAL RESULTS

The constants used in Section A.2 (Table A.3) for entrance length calculations were used in the calculations in Appendix B as well.

Table B.1: Reynolds Number Results for No Pins in Prototype

250 ml/min Tests							
Test	Flow rate (ml/min)	Flow rate (m ³ /s)	Velocity (m/s)	Re	ΔP (in. of H ₂ O)	ΔP (Pa)	K _L
1	271.38	4.52E-06	3.58E-03	148.55	0.95	236.40	3.71E+04
2	247.48	4.12E-06	3.26E-03	135.47	0.75	186.63	3.52E+04
3	263.18	4.39E-06	3.47E-03	144.06	0.85	211.51	3.53E+04
4	260.13	4.34E-06	3.43E-03	142.39	0.85	211.51	3.61E+04
5	247.41	4.12E-06	3.26E-03	135.43	0.85	211.51	3.99E+04
375 ml/min Tests							
Test	Flow rate (ml/min)	Flow rate (m ³ /s)	Velocity (m/s)	Re	ΔP (in. of H ₂ O)	ΔP (Pa)	K _L
1	381.87	6.36E-06	5.03E-03	209.03	1.25	311.05	2.46E+04
2	365.27	6.09E-06	4.81E-03	199.94	1.35	335.93	2.91E+04
3	373.60	6.23E-06	4.92E-03	204.50	1.35	335.93	2.78E+04
4	360.58	6.01E-06	4.75E-03	197.37	1.35	335.93	2.98E+04
5	368.68	6.14E-06	4.86E-03	201.81	1.35	335.93	2.85E+04
500 ml/min Tests							
Test	Flow rate (ml/min)	Flow rate (m ³ /s)	Velocity (m/s)	Re	ΔP (in. of H ₂ O)	ΔP (Pa)	K _L
1	479.80	8.00E-06	6.32E-03	262.64	1.55	385.70	1.93E+04
2	512.53	8.54E-06	6.75E-03	280.55	1.75	435.47	1.91E+04
3	504.84	8.41E-06	6.65E-03	276.34	1.90	472.80	2.14E+04
4	487.29	8.12E-06	6.42E-03	266.73	1.70	423.03	2.06E+04
5	479.48	7.99E-06	6.32E-03	262.46	1.65	410.59	2.06E+04
625 ml/min Tests							
Test	Flow rate (ml/min)	Flow rate (m ³ /s)	Velocity (m/s)	Re	ΔP (in. of H ₂ O)	ΔP (Pa)	K _L
1	629.41	1.05E-05	8.29E-03	344.53	2.35	584.77	1.70E+04
2	617.18	1.03E-05	8.13E-03	337.83	2.25	559.89	1.70E+04
3	629.90	1.05E-05	8.30E-03	344.79	2.30	572.33	1.67E+04
4	611.41	1.02E-05	8.06E-03	334.67	2.20	547.45	1.69E+04
5	622.47	1.04E-05	8.20E-03	340.73	2.25	559.89	1.67E+04
750 ml/min Tests							
Test	Flow rate (ml/min)	Flow rate (m ³ /s)	Velocity (m/s)	Re	ΔP (in. of H ₂ O)	ΔP (Pa)	K _L
1	747.90	1.25E-05	9.85E-03	409.39	2.75	684.31	1.41E+04
2	736.52	1.23E-05	9.70E-03	403.16	2.80	696.75	1.48E+04
3	764.36	1.27E-05	1.01E-02	418.40	2.60	646.98	1.28E+04
4	739.20	1.23E-05	9.74E-03	404.62	2.60	646.98	1.37E+04
5	744.98	1.24E-05	9.82E-03	407.79	2.60	646.98	1.35E+04
1000 ml/min Tests							
Test	Flow rate (ml/min)	Flow rate (m ³ /s)	Velocity (m/s)	Re	ΔP (in. of H ₂ O)	ΔP (Pa)	K _L
1	981.82	1.64E-05	1.29E-02	537.43	3.75	933.15	1.12E+04
2	967.00	1.61E-05	1.27E-02	529.32	3.90	970.48	1.20E+04
3	982.68	1.64E-05	1.29E-02	537.90	3.90	970.48	1.16E+04
4	1007.77	1.68E-05	1.33E-02	551.63	3.40	846.06	9.62E+03
5	989.24	1.65E-05	1.30E-02	541.49	3.65	908.27	1.07E+04

1125 ml/min Tests							
Test	Flow rate (ml/min)	Flow rate (m ³ /s)	Velocity (m/s)	Re	ΔP (in. of H ₂ O)	ΔP (Pa)	K _L
1	1133.31	1.89E-05	1.49E-02	620.35	3.70	920.71	8.28E+03
2	1115.85	1.86E-05	1.47E-02	610.79	3.85	958.03	8.88E+03
3	1126.67	1.88E-05	1.48E-02	616.72	3.75	933.15	8.49E+03
4	1117.21	1.86E-05	1.47E-02	611.54	3.80	945.59	8.75E+03
5	1147.34	1.91E-05	1.51E-02	628.03	3.85	958.03	8.40E+03
1250 ml/min Tests							
Test	Flow rate (ml/min)	Flow rate (m ³ /s)	Velocity (m/s)	Re	ΔP (in. of H ₂ O)	ΔP (Pa)	K _L
1	1251.08	2.09E-05	1.65E-02	684.82	4.00	995.36	7.34E+03
2	1245.72	2.08E-05	1.64E-02	681.89	4.10	1020.2	7.59E+03
3	1249.89	2.08E-05	1.65E-02	684.17	4.10	1020.2	7.54E+03
4	1253.78	2.09E-05	1.65E-02	686.30	4.10	1020.2	7.49E+03
5	1270.98	2.12E-05	1.67E-02	695.71	4.15	1032.6	7.38E+03

Table B.2: Reynolds Number Results for Pin 1 in Prototype

250 ml/min Tests							
Test	Flow rate (ml/min)	Flow rate (m ³ /s)	Velocity (m/s)	Re	ΔP (in. of H ₂ O)	ΔP (Pa)	K _L
1	267.75	4.46E-06	3.53E-03	146.56	0.85	211.51	3.41E+04
2	247.27	4.12E-06	3.26E-03	135.35	0.85	211.51	3.99E+04
3	242.96	4.05E-06	3.20E-03	132.99	0.85	211.51	4.14E+04
4	249.62	4.16E-06	3.29E-03	136.64	0.95	236.40	4.38E+04
5	262.54	4.38E-06	3.46E-03	143.71	0.95	236.40	3.96E+04
375 ml/min Tests							
Test	Flow rate (ml/min)	Flow rate (m ³ /s)	Velocity (m/s)	Re	ΔP (in. of H ₂ O)	ΔP (Pa)	K _L
1	382.99	6.38E-06	5.05E-03	209.64	1.25	311.05	2.45E+04
2	383.97	6.40E-06	5.06E-03	210.18	1.30	323.49	2.53E+04
3	389.55	6.49E-06	5.13E-03	213.23	1.25	311.05	2.37E+04
4	375.58	6.26E-06	4.95E-03	205.59	1.35	335.93	2.75E+04
5	389.24	6.49E-06	5.13E-03	213.06	1.30	323.49	2.46E+04
500 ml/min Tests							
Test	Flow rate (ml/min)	Flow rate (m ³ /s)	Velocity (m/s)	Re	ΔP (in. of H ₂ O)	ΔP (Pa)	K _L
1	502.29	8.37E-06	6.62E-03	274.94	1.90	472.80	2.16E+04
2	502.95	8.38E-06	6.63E-03	275.30	2.10	522.56	2.38E+04
3	501.89	8.36E-06	6.61E-03	274.73	2.10	522.56	2.39E+04
4	505.11	8.42E-06	6.66E-03	276.49	1.90	472.80	2.14E+04
5	513.48	8.56E-06	6.77E-03	281.07	1.90	472.80	2.07E+04
625 ml/min Tests							
Test	Flow rate (ml/min)	Flow rate (m ³ /s)	Velocity (m/s)	Re	ΔP (in. of H ₂ O)	ΔP (Pa)	K _L
1	628.80	1.05E-05	8.28E-03	344.19	2.30	572.33	1.67E+04
2	623.15	1.04E-05	8.21E-03	341.10	2.50	622.10	1.85E+04
3	625.60	1.04E-05	8.24E-03	342.44	2.40	597.22	1.76E+04
4	632.84	1.05E-05	8.34E-03	346.40	2.50	622.10	1.79E+04
5	618.74	1.03E-05	8.15E-03	338.69	2.50	622.10	1.88E+04
750 ml/min Tests							
Test	Flow rate (ml/min)	Flow rate (m ³ /s)	Velocity (m/s)	Re	ΔP (in. of H ₂ O)	ΔP (Pa)	K _L
1	743.60	1.24E-05	9.80E-03	407.03	3.05	758.96	1.58E+04
2	748.60	1.25E-05	9.86E-03	409.77	3.50	870.94	1.79E+04
3	766.72	1.28E-05	1.01E-02	419.69	3.10	771.40	1.51E+04
4	728.96	1.21E-05	9.60E-03	399.02	3.00	746.52	1.62E+04
5	724.82	1.21E-05	9.55E-03	396.75	3.00	746.52	1.64E+04
1000 ml/min Tests							
Test	Flow rate (ml/min)	Flow rate (m ³ /s)	Velocity (m/s)	Re	ΔP (in. of H ₂ O)	ΔP (Pa)	K _L
1	984.37	1.64E-05	1.30E-02	538.82	5.80	1443.27	1.72E+04
2	979.71	1.63E-05	1.29E-02	536.28	5.00	1244.20	1.50E+04
3	995.79	1.66E-05	1.31E-02	545.08	5.20	1293.97	1.51E+04
4	965.43	1.61E-05	1.27E-02	528.46	4.90	1219.32	1.51E+04
5	979.42	1.63E-05	1.29E-02	536.12	5.20	1293.97	1.56E+04

Table B.3: Reynolds Number Results for Pin 2 in Prototype

250 ml/min Tests							
Test	Flow rate (ml/min)	Flow rate (m ³ /s)	Velocity (m/s)	Re	ΔP (in. of H ₂ O)	ΔP (Pa)	K _L
1	258.40	4.31E-06	3.40E-03	141.45	0.80	199.07	3.44E+04
2	250.27	4.17E-06	3.30E-03	136.99	0.85	211.51	3.90E+04
3	233.15	3.89E-06	3.07E-03	127.62	0.80	199.07	4.23E+04
4	238.35	3.97E-06	3.14E-03	130.47	0.85	211.51	4.30E+04
5	226.38	3.77E-06	2.98E-03	123.92	0.95	236.40	5.32E+04
375 ml/min Tests							
Test	Flow rate (ml/min)	Flow rate (m ³ /s)	Velocity (m/s)	Re	ΔP (in. of H ₂ O)	ΔP (Pa)	K _L
1	396.03	6.60E-06	5.22E-03	216.78	1.35	335.93	2.47E+04
2	373.80	6.23E-06	4.93E-03	204.61	1.20	298.61	2.47E+04
3	376.08	6.27E-06	4.96E-03	205.86	1.25	311.05	2.54E+04
4	363.28	6.05E-06	4.79E-03	198.85	1.25	311.05	2.72E+04
5	376.54	6.28E-06	4.96E-03	206.11	1.25	311.05	2.53E+04
500 ml/min Tests							
Test	Flow rate (ml/min)	Flow rate (m ³ /s)	Velocity (m/s)	Re	ΔP (in. of H ₂ O)	ΔP (Pa)	K _L
1	471.35	7.86E-06	6.21E-03	258.01	1.85	460.35	2.39E+04
2	487.67	8.13E-06	6.43E-03	266.94	1.80	447.91	2.17E+04
3	486.01	8.10E-06	6.40E-03	266.03	1.75	435.47	2.13E+04
4	487.75	8.13E-06	6.43E-03	266.99	1.80	447.91	2.17E+04
5	521.14	8.69E-06	6.87E-03	285.26	1.85	460.35	1.96E+04
625 ml/min Tests							
Test	Flow rate (ml/min)	Flow rate (m ³ /s)	Velocity (m/s)	Re	ΔP (in. of H ₂ O)	ΔP (Pa)	K _L
1	631.41	1.05E-05	8.32E-03	345.62	2.30	572.33	1.66E+04
2	629.48	1.05E-05	8.29E-03	344.57	2.30	572.33	1.67E+04
3	635.47	1.06E-05	8.37E-03	347.84	2.30	572.33	1.64E+04
4	630.88	1.05E-05	8.31E-03	345.33	2.30	572.33	1.66E+04
5	629.78	1.05E-05	8.30E-03	344.73	2.30	572.33	1.67E+04
750 ml/min Tests							
Test	Flow rate (ml/min)	Flow rate (m ³ /s)	Velocity (m/s)	Re	ΔP (in. of H ₂ O)	ΔP (Pa)	K _L
1	757.55	1.26E-05	9.98E-03	414.67	2.95	734.08	1.48E+04
2	762.19	1.27E-05	1.00E-02	417.21	3.10	771.40	1.53E+04
3	772.65	1.29E-05	1.02E-02	422.93	3.10	771.40	1.49E+04
4	764.41	1.27E-05	1.01E-02	418.43	3.20	796.29	1.57E+04
5	758.06	1.26E-05	9.99E-03	414.95	3.10	771.40	1.55E+04
1000 ml/min Tests							
Test	Flow rate (ml/min)	Flow rate (m ³ /s)	Velocity (m/s)	Re	ΔP (in. of H ₂ O)	ΔP (Pa)	K _L
1	970.58	1.62E-05	1.28E-02	531.28	4.70	1169.5	1.43E+04
2	992.30	1.65E-05	1.31E-02	543.17	4.80	1194.4	1.40E+04
3	1010.65	1.68E-05	1.33E-02	553.21	4.90	1219.3	1.38E+04
4	1005.33	1.68E-05	1.32E-02	550.30	4.70	1169.5	1.34E+04
5	983.61	1.64E-05	1.30E-02	538.41	4.50	1119.7	1.34E+04

Table B.4: Reynolds Number Results for Pin 3 in Prototype

250 ml/min Tests							
Test	Flow rate (ml/min)	Flow rate (m ³ /s)	Velocity (m/s)	Re	ΔP (in. of H ₂ O)	ΔP (Pa)	K _L
1	254.26	4.24E-06	3.35E-03	139.18	0.85	211.51	3.78E+04
2	245.50	4.09E-06	3.23E-03	134.38	0.85	211.51	4.05E+04
3	240.32	4.01E-06	3.17E-03	131.55	0.85	211.51	4.23E+04
4	249.38	4.16E-06	3.29E-03	136.50	0.85	211.51	3.93E+04
5	225.21	3.75E-06	2.97E-03	123.27	0.90	223.96	5.10E+04
500 ml/min Tests							
Test	Flow rate (ml/min)	Flow rate (m ³ /s)	Velocity (m/s)	Re	ΔP (in. of H ₂ O)	ΔP (Pa)	K _L
1	490.94	8.18E-06	6.47E-03	268.73	1.70	423.03	2.03E+04
2	510.23	8.50E-06	6.72E-03	279.29	1.80	447.91	1.99E+04
3	481.63	8.03E-06	6.35E-03	263.64	1.60	398.14	1.98E+04
4	504.73	8.41E-06	6.65E-03	276.28	1.65	410.59	1.86E+04
5	489.28	8.15E-06	6.45E-03	267.82	1.65	410.59	1.98E+04
750 ml/min Tests							
Test	Flow rate (ml/min)	Flow rate (m ³ /s)	Velocity (m/s)	Re	ΔP (in. of H ₂ O)	ΔP (Pa)	K _L
1	762.17	1.27E-05	1.00E-02	417.20	2.75	684.31	1.36E+04
2	752.32	1.25E-05	9.91E-03	411.80	2.75	684.31	1.40E+04
3	732.99	1.22E-05	9.66E-03	401.23	2.70	671.87	1.44E+04
4	740.69	1.23E-05	9.76E-03	405.44	2.75	684.31	1.44E+04
5	741.40	1.24E-05	9.77E-03	405.83	2.60	646.98	1.36E+04
1000 ml/min Tests							
Test	Flow rate (ml/min)	Flow rate (m ³ /s)	Velocity (m/s)	Re	ΔP (in. of H ₂ O)	ΔP (Pa)	K _L
1	1006.67	1.68E-05	1.33E-02	551.03	3.85	958.03	1.09E+04
2	1021.38	1.70E-05	1.35E-02	559.08	3.90	970.48	1.07E+04
3	992.78	1.65E-05	1.31E-02	543.43	3.75	933.15	1.09E+04
4	1007.47	1.68E-05	1.33E-02	551.47	3.85	958.03	1.09E+04
5	998.03	1.66E-05	1.31E-02	546.30	3.80	945.59	1.10E+04
1125 ml/min Tests							
Test	Flow rate (ml/min)	Flow rate (m ³ /s)	Velocity (m/s)	Re	ΔP (in. of H ₂ O)	ΔP (Pa)	K _L
1	1115.49	1.86E-05	1.47E-02	610.60	3.95	982.92	9.12E+03
2	1107.38	1.85E-05	1.46E-02	606.16	3.90	970.48	9.14E+03
3	1128.51	1.88E-05	1.49E-02	617.72	3.95	982.92	8.91E+03
4	1110.73	1.85E-05	1.46E-02	607.99	3.70	920.71	8.62E+03
5	1130.87	1.88E-05	1.49E-02	619.02	3.85	958.03	8.65E+03
1250 ml/min Tests							
Test	Flow rate (ml/min)	Flow rate (m ³ /s)	Velocity (m/s)	Re	ΔP (in. of H ₂ O)	ΔP (Pa)	K _L
1	1258.08	2.10E-05	1.66E-02	688.65	4.50	1119.78	8.17E+03
2	1276.13	2.13E-05	1.68E-02	698.53	4.30	1070.01	7.59E+03
3	1249.46	2.08E-05	1.65E-02	683.93	4.45	1107.34	8.19E+03
4	1254.26	2.09E-05	1.65E-02	686.56	4.30	1070.01	7.85E+03
5	1241.63	2.07E-05	1.64E-02	679.65	4.40	1094.90	8.20E+03

APPENDIX C

UNCERTAINTY ANALYSIS

For each instrument used, the uncertainty is desired. The propagation of the uncertainty of values obtained with these instruments that are used to calculate other entities is then desired. The instrument uncertainty is given by u_o . To calculate u_o , simply half the instrument resolution as shown in Equation C.2 (Beasley and Figliola 183).

$$u_{o,y} = \pm \frac{1}{2}(\text{resolution}) \quad (\text{C.1})$$

The propagation of uncertainty to a result, R , that is a function of several independent variables shown in Equation C.3 is given by Equation C.4 (Beasley and Figliola 180).

$$R = f(y_1, y_2, \dots, y_L) \quad (\text{C.2})$$

$$u_R = \pm \sqrt{\sum_{i=1}^L (\theta_i u_{y_i})^2} \quad (\text{C.3})$$

θ_i is given by Equation C.5 below (Beasley and Figliola 180). In this equation, \bar{y} is the point at which the uncertainty is being calculated.

$$\theta_i = \left. \frac{\partial R}{\partial y_i} \right|_{y=\bar{y}} \quad i=1,2,\dots,L \quad (\text{C.4})$$

For example, the formula for the uncertainty of the loss coefficient K_L , given in Equation 1.4, is derived below. Equation C.6.

$$K_L = \frac{2\Delta P}{\rho V^2} = \frac{2\Delta P \frac{\pi^2}{16} D^4}{\rho Q^2} \quad (\text{C.5})$$

$$\frac{\partial K}{\partial D} = \frac{\pi^2 \Delta P D^3}{2\rho Q^2} \quad (\text{C.6})$$

$$\frac{\partial K}{\partial Q} = -\frac{\pi^2 \Delta P D^4}{2\rho Q^3} \quad (\text{C.7})$$

$$\frac{\partial K}{\partial \Delta P} = \frac{\pi^2 D^4}{8\rho Q^2} \quad (\text{C.8})$$

$$u_{K_L} = \pm \sqrt{\left(\frac{\partial K_L}{\partial D} u_D\right)^2 + \left(\frac{\partial K_L}{\partial Q} u_Q\right)^2 + \left(\frac{\partial K_L}{\partial \Delta P} u_{\Delta P}\right)^2} \quad (\text{C.9})$$

The uncertainties for the instruments used in the experiments and the uncertainty analysis are shown below.

Table C.1: Flow Measurement Uncertainty Summary

Flow Uncertainty	
$u_{\text{avg}}(\pm)$ (ml/min)	21.16
$u_{\text{min}}(\pm)$ (ml/min)	4.71
$u_{\text{max}}(\pm)$ (ml/min)	35.88

Table C.2: Pressure and Diameter Measurement Uncertainty Summary

Slack Tube Manometer	
$u_0(\pm)$ (in. of H ₂ O)	0.07
High Flow Uncertainty	
$u_{\Delta P}(\pm)$ (in. of H ₂ O)	0.07
$u_{\Delta P}(\pm)$ (Pa)	17.67
Uncertainty in Diameter	
$u_D(\pm)$ (in.)	5.00E-04
$u_D(\pm)$ (m)	1.27E-05

Table C.3: Loss Coefficient Uncertainty Summary

	Flow Rate (ml/min)	ΔP (Pa)	$\partial K/\partial D$	$\partial K/\partial Q$	$\partial K/\partial \Delta P$	$u_{K_L}(\pm)$	K_L
max	1115.85	958.03	8.85E+05	-9.55E+08	9.27E+00	5.94E+02	8.88E+03
min	629.78	572.33	1.66E+06	-3.17E+09	2.91E+01	5.72E+02	1.67E+04

Table C.4: Reynolds Number Uncertainty Summary

	$\partial \text{Re}/\partial D$	$\partial \text{Re}/\partial Q$	$u_{\text{Re}}(\pm)$	Re
max	-15219.61	3.28E+07	21.06	610.79
min	-8589.84	3.28E+07	5.01	344.73

APPENDIX D

DIMENSIONED DRAWINGS OF PROTOTYPE

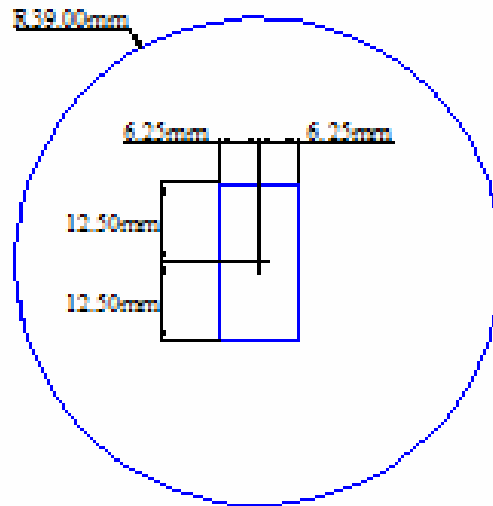


Figure D.1: Dimensions for Top Layer of Valve Prototype

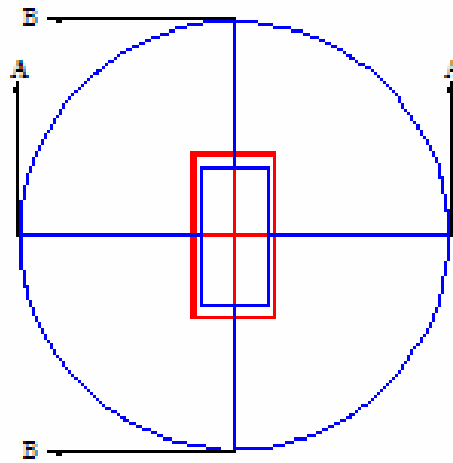


Figure D.2: Section View of Prototype

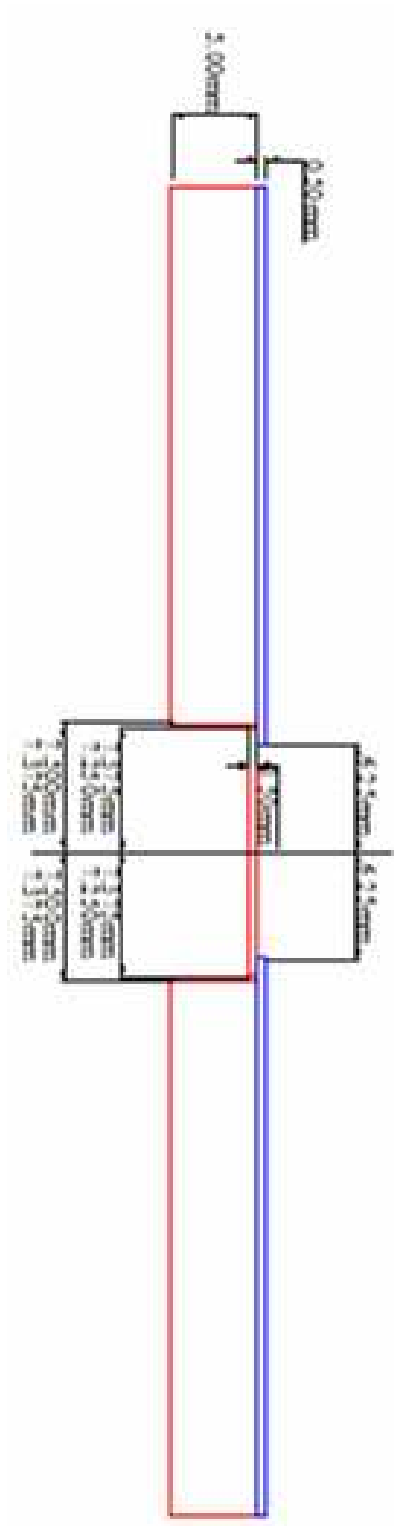


Figure D.3: Section A-A View of Prototype

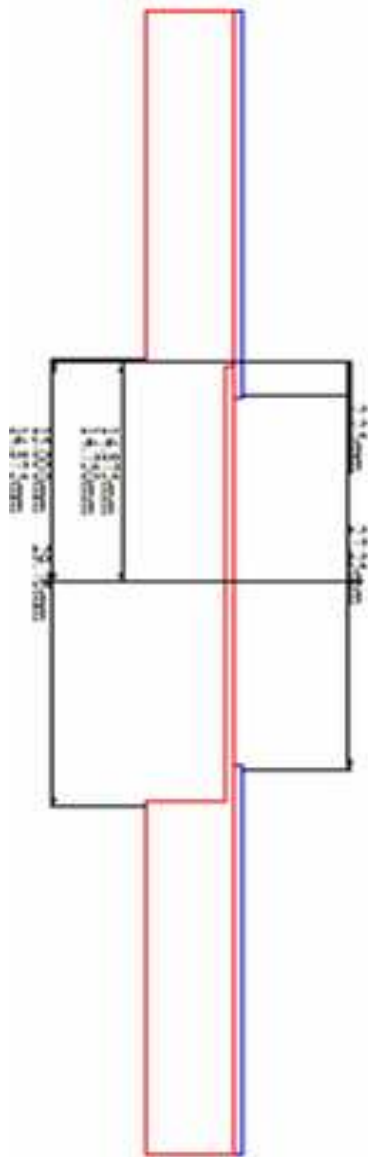


Figure D.4: Section B-B View of Prototype

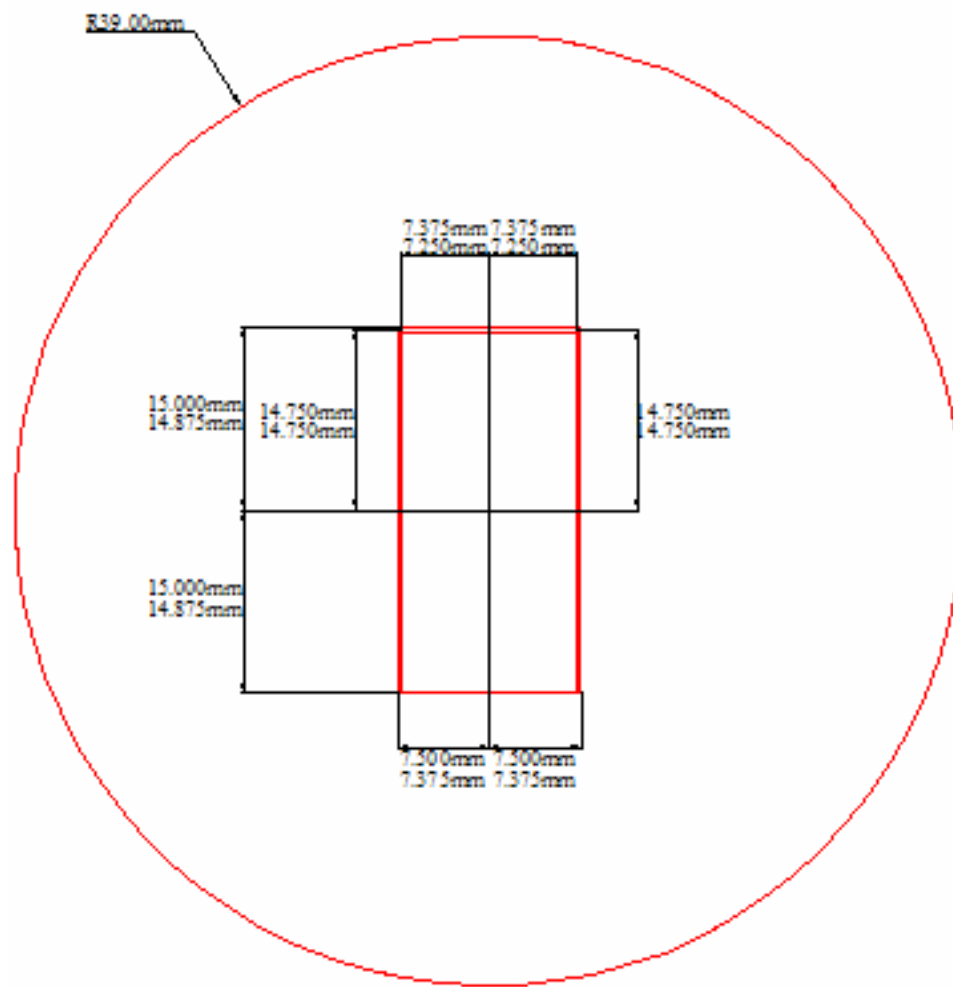


Figure D.5: Dimensions for Bottom Layer of Prototype

APPENDIX E

EQUIPMENT SPECIFICATIONS

E.1 Flowmeter Specifications

Graphics obtained from: <http://www.omega.com/Green/pdf/FLR1000.pdf>.

GAS/LIQUID FLOW SENSORS WITH 0 TO 5 VDC OUTPUT

FLR1000 Series

\$184

Basic Unit



- ✓ 0 to 5 Vdc Linear Output Signal
- ✓ Highly Repeatable — Excellent Resolution
- ✓ Very Stable
- ✓ No Zero Drift
- ✓ Power Input 12 Vdc
- ✓ Ranges from 20 to 100 ml/min, 1 to 5 L/min

FLR1000 Series flow sensors are capable of measuring extremely low flowrates from 20 ml/min to 5 liters/min. These sensors are suitable for a wide variety of industrial, commercial and laboratory flow applications. FLR1000 series flow sensors operate on 12 Vdc power and have been especially designed for incorporation into data acquisition systems that supply 12.5 Vdc to sensors and receive 0 to 5 Vdc linear signals from such sensors.

Because of the low cost of these flow sensors, it is anticipated that these units will replace conventional glass tube and ball flow meters in many applications where an electrical signal proportional to flowrate is considered desirable.

The FLR1000 Series uses a Pelton-type turbine wheel to determine the flowrate of the gas. Rotation rate of the turbine wheel is linear over a large dynamic range. The electro-optical system consists of a diode emitting energy in the infrared spectrum. Light energy is alternatively reflected and absorbed from "spokes" deposited upon the small turbine wheel. This reflected light energy is detected by means of a photo-diode. Thus, as the turbine wheel rotates in response to gas flowrate, electrical pulses are generated.

Processing circuitry provides a dc voltage output proportional to the flow rate. For example, output signal is 1.0 Vdc at 20% of rated flow, 2.5 Vdc at 50% of rated flow, 4.0 Vdc at 80% of rated flow and 5.0 Vdc at 100% of rated flow. Sensors can handle 20% above their rated flow without being damaged.

SPECIFICATIONS

Accuracy: $\pm 3\%$ full scale
Output Signal: 0 to 5 Vdc, adjustable $\pm 20\%$ (typical)

Power Requirement:
12.5 ± 2 Vdc regulated 30 mA (typical) for FLR1000 Series
Standard Sensor Material: 40% glass filled polyphenylene sulphide, glass window, stainless steel bearing support; sapphire shaft and bearing; Viton® rubber "O"-rings standard
Pressure Rating: 40 psi at 20°C (68°F) for gas, 100 psi for liquid, 500 psi for brass units using liquid services
Temperature Rating:
0 to 50°C (32 to 122°F)

Temperature Sensitivity: $\pm 0.2\%/^{\circ}\text{C}$
Linearity: $\pm 3\%$ full scale
Repeatability: $\pm 0.5\%$ full scale from 50 to 100% of rated max flow for gas; $\pm 0.2\%$ FS for liquid
Required Cable Assembly:
0.9 m (3') cable length
Dimensions: 59.7 x 41.9 x 38.1 mm (2.35 x 1.65 x 1.50")
Pressure Sensitivity: $\pm 0.07\%$ mm Hg. (using air at 1 to 3 atm.)
Mounting: Holes for #4 screw provided

HIGHLIGHTED MODELS STOCKED FOR FAST DELIVERY!

To Order (Specify Model Number)

Model No.	Price	Flow Range/Gas	Max ΔP PSI	Acetal Tube Fittings
FLR1001	\$184	20 to 100 ml/min	1.5" H ₂ O	1/8"
FLR1002	184	40 to 200 ml/min	6.6" H ₂ O	1/8"
FLR1003	184	100 to 500 ml/min	1.45" H ₂ O	1/8"
FLR1004	184	200 to 1000 ml/min	0.9" H ₂ O	1/8"
FLR1005	184	0.4 to 2.0 L/min	0.4" H ₂ O	1/8"
FLR1006	184	1.0 to 5.0 L/min	0.35" H ₂ O	1/8"
Model No.	Price	Flow Range/Liquid	ΔP PSI	
FLR1007	\$184	13 to 100 ml/min	10	1/8"
FLR1008	184	20 to 200 ml/min	10	1/8"
FLR1009	184	50 to 500 ml/min	10	1/8"
FLR1010	184	60 to 1000 ml/min	6	1/8"
FLR1011	184	0.1 to 2.0 l/min	6	1/8"
FLR1012	224	0.2 to 5.0 l/min	6	3/8"

Units come with 0.9 m (3') cable and operator's manual

Note: Liquid flow sensors (Models FLR1007 through FLR1012) are available with brass instead of glass-filled polyphenylene; to order, add suffix "-BR" to model number and add \$150 to price. All units are also available with pulse output in addition to 0.5 V output; add suffix "-P" and \$40.

Ordering Example: FLR1012, liquid flow sensor, 0.2 to 5.0 l/min, \$224.

Accessories

Model No.	Price	Description
FLR1000-PW	\$60	Power supply
FLR1000-230PW	60	230 V power supply with European Connector
DPF51	145	Panel meter

Figure E.1: Flow Meter Specs for FLR 1012


E.2 Thermocouple Specifications

Graphics obtained from: <http://www.omega.com/Temperature/pdf/TC-NPT.pdf>.

Pipe Plug Probe

- ✓ Rugged 304SS Design with Strain Relief Spring
- ✓ Fiberglass Leads Protected with Steel Overbraiding
- ✓ Stripped Leads, Standard. SMPW Connectors, Optional
- ✓ 1/4 NPT Mountings
- ✓ Choice J, K, T or E Thermocouple Types
- ✓ Grounded, Ungrounded or Exposed Junctions

TC-(*)-NPT Series
\$34
Basic Unit



TC-K-NPT-U-72, \$39
Pipe Plug Probe With Ungrounded Junction, Stripped Wire Leads and Stainless Steel Overbraid Shown

Ordering Example: TC-K-NPT-G-72 is a grounded pipe plug probe with stripped leads, \$34

* Specify calibration: J, K, T or E
** Other lengths available, consult Sales Department
For exposed junction, replace G with E in model number, same price
For subminiature connector, add suffix "-SMPW" and \$5 to price
For standard connector, add suffix "-OSTW" and \$5 to price

1/4 and 1/8 NPT fitting — Single and Dual Thermocouple Configurations

Figure E.2: Thermocouple Specs for TC-J-NPT

E.3 Manometer Specifications

Model number 3986K14

Graphics obtained from: <http://www.mcmaster.com/>, catalog page 528.

Table E.1: Manometer Specs for 3986K14

- Maximum Pressure: 50 psi
- Tube rolls up for portability
- U-Tube Material: Flexible vinyl
- Connections: Barbed for 3/16" ID tubing
- Tubing Connectors: Nylon
- Furnished with magnetic mounting clips; carrying case; and 3/4 oz. of concentrated, green indicating liquid (specific gravity of 1)

Pressure Range, inches of H ₂ O	Scale, inches of H ₂ O*	Each	
0-8	4-0-4	3986K11	\$46.06
0-12	6-0-6	3986K12	50.70
0-16	8-0-8	3986K13	51.24
0-24	12-0-12	3986K14	53.68
0-30	15-0-15	3986K15	56.14
0-36	18-0-18	3986K16	56.68
0-48	24-0-24	3986K17	67.59
0-60	30-0-30	3986K18	70.86
0-72	36-0-36	3986K19	70.86
0-120	60-0-60	3986K2	75.76
*Figure intervals are 1" of H ₂ O; graduation marks are 0.1" of H ₂ O.			

APPENDIX F

MATERIAL PROPERTIES OF ACETRON GP

Obtained from:

<http://www.quadrantepp.matweb.com/SpecificMaterialNew.asp?bassnum=P1SM00&group=General>.

Table F.1: Material Properties of Acetron GP Acetal

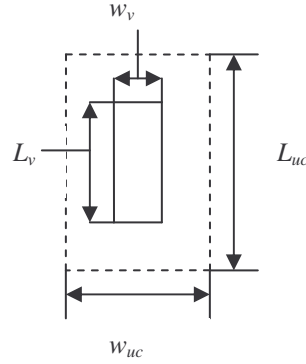
MECHANICAL PROPERTIES	ENGLISH VALUES	COMMENTS	METRIC VALUES
Specific Gravity	1.41	ASTM D792	1.41
Tensile Strength, psi	9500	ASTM D638	66 Mpa
Tensile Modulus, psi	400000	ASTM D638	2,758 Mpa
Elongation, %	30	ASTM D638	30 %
Flexural Strength, psi	12000	ASTM D790	83 Mpa
Flexural Modulus, psi	400000	ASTM D790	2,758 Mpa
Shear Strength, psi	8000	ASTM D732	55 Mpa
Compressive Strength, psi	15000	ASTM D695, 10% Def.	103 Mpa
Compressive Modulus, psi	400000	ASTM D695	2,758 Mpa
Hardness, Rockwell M	88	ASTM D785	88
Hardness, Rockwell R	120	ASTM D785	120
Hardness, Durometer, Shore D Scale	85	ASTM D2240	85
Izod Impact (Notched), ft-lb/in	1	ASTM D256 Type A	53 J/m
Coefficient of Friction, Dynamic	0.25	Dry vs. Steel, PTM55007	0.25
Limiting PV, psi-fpm	2700	PTM55007	0.09 Mpa-m/sec
k (wear) factor, 10 ⁻¹⁰ in ³ -min/lb-ft-hr	200	PTM55007	200 10 ⁻¹⁰ in ³ -min/lb-ft-hr
THERMAL PROPERTIES	ENGLISH VALUES	COMMENTS	METRIC VALUES
Coefficient of Thermal Expansion, 10E-4/°F	0.54	ASTM E831 (TMA)	0.97 10 ⁻⁴ /K
Deflection Temperature 264 psi, °F	220	ASTM D648	104 °C
Melting Point (Crystalline) Peak, °F	335	ASTM D3418	168 °C
Continuous Service in Air (Max), °F	180	Without Load	82 °C
Thermal Conductivity, BTU-in/hr-ft ² -°F	1.6		0.23 W/m-K
ELECTRICAL PROPERTIES	VALUES	COMMENTS	METRIC VALUES
Dielectric Strength, Short Term, Volts/mil	420	ASTM D149(2)	17 kV/mm
Surface Resistance, Ohm/Square	1E+15	EOS/ESD S11.11	1E+15 Ohm/Square
Dielectric Constant, 1 MHz	3.8	ASTM D150(2)	3.8
Dissipation Factor, 1 MHz	0.005	ASTM D150(2)	0.005

CHEMICAL PROPERTIES	ENGLISH VALUES	COMMENTS	METRIC VALUES
Water Absorption Immersion, 24 hr., %	0.2	ASTM D570	0.2 %
Water Absorption Immersion Sat, %	0.9	ASTM D570	0.9 %
Acids, Weak (acetic, dilute HCl)	2	Limited Service	2
Acids, Strong (conc. HCl or sulfuric)	1	Unacceptable	1
Alkalies, Weak (dilute NaOH)	3	Acceptable Service	3
Alkalies, Strong (conc. NaOH)	1	Unacceptable	1
Hydrocarbons, Aromatic (toluene)	3	Acceptable Service	3
Hydrocarbons, Aliphatic (gasoline)	3	Acceptable Service	3
Ketones, Esters (acetone)	3	Acceptable Service	3
Ethers (diethyl ether, THF)	3	Acceptable Service	3
Chlorinated Solvents (methylene chloride)	2	Limited Service	2
Alcohols (methanol, anti-freeze)	3	Acceptable Service	3
Inorganic Salt Solutions (NaCl, KCl)	3	Acceptable Service	3
Continuous Sunlight	2	Limited Service	2
Steam	2	Limited Service	2
COMPLIANCE	ENGLISH VALUES	COMMENTS	METRIC VALUES
Flammability, UL94 (5=V-0; 4=V-1; 3=V-2; 1=HB)	1 (HB)	UL94	1
FDA (1=Yes)	1	Compliant	1
USDA (1=Yes)	1	Compliant	1
NSF (1=Yes)	1	Compliant	1
3A-Dairy (1=Yes)	1	Compliant	1
Canada AG (1=Yes)	1	Compliant	1
USP Class VI (1=Yes)	0	Not Compliant	0

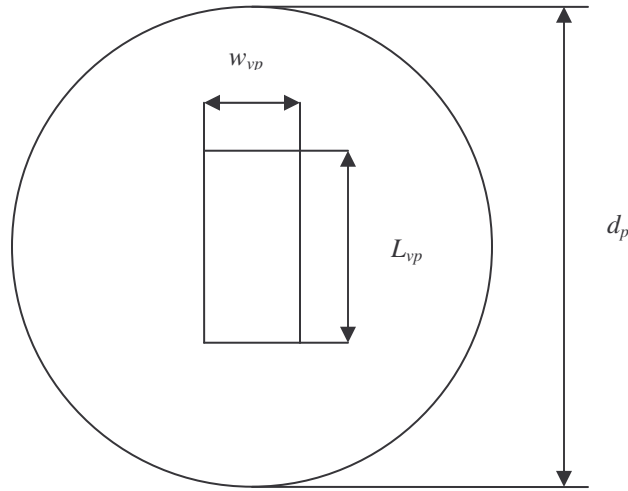
APPENDIX G

REYNOLDS NUMBER AND GEOMETRIC SCALING

Equating the two following geometries and Reynolds numbers (figures not drawn to scale):



(a)



(b)

Figure G.1: (a) Unit Cell for Smart Valve Layer, (b) Valve Prototype

In order to simulate a unit cell of the felt (shown above) with the prototype, the Reynolds number and geometry must be equated.

$$\text{Re}_f = \text{Re}_p \quad (\text{G.1})$$

$$\frac{\rho_f V_{f,\max} d_{h,uc}}{\mu_f} = \frac{\rho_p V_{p,\max} d_p}{\mu_p} \quad (\text{G.2})$$

$$d_{h,uc} = \frac{2L_{uc}w_{uc}}{L_{uc} + w_{uc}} \quad (G.3)$$

For similar geometries, the ratio of the hydraulic diameters is required to be equal. This is shown in the equations below.

$$\frac{d_{h,v}}{d_{h,uc}} = \frac{d_{h,vp}}{d_p} \quad (G.4)$$

$$\text{where } d_{h,v} = \frac{2L_vw_v}{L_v + w_v} \quad (G.5)$$

$$\text{and } d_{h,vp} = \frac{2L_{vp}w_{vp}}{L_{vp} + w_{vp}} \quad (G.6)$$

For the felt, the values L_v , w_v , $V_{f,max}$, ρ_f , and μ_f are known. For the prototype, the values L_{vp} , w_{vp} , d_p , ρ_p , and μ_p are known. Thus, $d_{h,v}$ and $d_{h,vp}$ can be found from Equations G.5 and G.6.

The value $d_{h,uc}$ can then be found and from Equation G.4. The dimension L_{uc} and w_{uc} can be chosen to satisfy $d_{h,uc}$. The applicable Reynolds number for flow in the smart felt is found and translated into the Reynolds number for pipe flow for the experimental simulation.

REFERENCES

- Ashworth, Gordon. U.S. Patent No. 4,162,190, Scapa-Poritt Limit: July 24, 1979.
- Beasley, Donald E. and Richard Figliola. *Theory and Design for Mechanical Measurements*. John Wiley and Sons, Inc.: New York, NY, 1995.
- Beck, David A. U.S. Patent No. 6,616,812, Voith Paper Patent GmbH: September 9, 2003.
- Bermond, C. "Establishing the Scientific Base for Energy Efficiency in Emerging Pressing and Drying Technologies." *Applied Thermal Engineering* 17.8-17.10 Aug.-Oct. 1997: 901-910.
- Blevins, Robert D. *Applied Fluid Dynamics Handbook*. Van Nostrand Reinhold Co. Inc.: New York, NY, 1984.
- Busker, Leroy H. and Robert A. Daane. U.S. Patent No. 3,840,429, Beloit Corporation: October 8, 1974.
- Ceckler, William H., et al. "Rewetting in the expansion side of press nips." *Tappi Journal* March 1988: 151-155.
- Dewitt, David P. and Frank P. Incropera. Fundamentals of Heat and Mass Transfer, 4th ed. John Wiley and Sons, Inc.: New York, NY, 1996
- Eklund, Nils O., et al. U.S. Patent No. 5,232,768, Nordiskafilt AB: August 3, 1993.
- El-Hosseiny, Farouk. "An Equation for Press Felt Compression." *Tappi Journal* August 1991: 193-196.
- Eschmann, Sylvester. U.S. Patent No. 5,204,171, Thomas Joseph Heimbach GmbH: April 20, 1993.
- Fitton, G.R. "An Engineered Press Nip." *Paper Technology and Industry* 26.2 March 1985: 50-54.
- Greenkorn, Robert A. *Flow Phenomena in Porous Media*. Marcel Dekker, Inc.: New York, NY, 1983.
- Hok. B., et al. "A Batch-Fabricated Non-Reverse Valve with Cantilever Beam Manufactured by Micromachining of Silicon." *Sensors and Actuators* 18.3-18.4 July 1989: 389-396.

<http://www.mcmaster.com/>

<http://www.omega.com/Green/pdf/FLR1000.pdf>

<http://www.omega.com/Temperature/pdf/TC-NPT.pdf>

<http://www.quadrantepp.matweb.com/SpecificMaterialNew.asp?bassnum=P1SM00&group=General>.

Ibrahim, Ahmed A. "Survey: Understanding Rewetting Phenomenon in the Pressing Operation." *Pulp and Paper Canada* 82.2 Feb. 1981: 73-76.

Johnson, Michael C. and Gary V. Schultz. U.S. Patent No. 5,372,876, Appleton Mills: December 13, 1994.

Joyce, Michael J. U.S. Patent No. 6,592,636, Albany International Corporation: July 15, 2003.

Kreith, Frank. *Fluid Mechanics*. CRC Press: Boca Raton, Florida, 2000.

Liu, Thomas J. and Cyrille M. Cottigny. U.S. Patent No. 4,199,401, Asten Group, Inc.: April 22, 1980.

Lundstrom, Kristian. U.S. Patent No. 4,588,475, Tamfelt Oy AB: May 13, 1986.

Munson, Bruce R., et al. Fundamentals of Fluid Mechanics. John Wiley and Sons, Inc.: New York, NY, 2002.

Nyberg, Esko. U.S. Patent No. 4,988,409, Tamfelt Oy AB: January 29, 1991.

Orthwein, William. *Machine Component Design*, West Publishing Co.: St. Paul, MN, 1990.

Palokangas, Antti. "Vacuum Felts Increase Sheet Dryness by Preventing Rewetting at Press Nip." *Pulp and Paper* 64.8 Aug. 1990: 101-104.

Plaisted, W.E. "Press Felt Properties Affecting Optimum Sheet Dewatering." *Pulp and Paper Canada* 82.7 July 1981: 42-45.

Rudman, Isaak. Personal interview. 24 August 2004.

Rudman, Isaak. Personal interview. 30 August 2004.

Shaw, Monica. "Papermakers Question Clothing Suppliers on Design, Service, Price." *Pulp and Paper* 74.11 Nov. 2000: 57-61.

Smart, Frederick R. "Water Removal Performance on a Grooved Second Press." *Paper Technology and Industry* 16.3 June 1975: 172-178.

Swain, Gregory E. "Behavior of Press Felts in Compression." *Engineering Conference, Proceedings of the Technical Association of the Pulp and Paper Industry* 1980: 53-61.

Szikla, Zoltan. "Role of Felt in Wet Pressing: Part 2. Movement of water during the separation of paper from felt." *Paper and Timber* 73.2 1991: 160-166.

Wilder, John E. "Paper Capillarity and Rewetting During Pressing." *Tappi* 51.2 Feb. 1968: 104-109.

Wiseman, Nick. "The Effect of Felt Properties on the Pressing of Paper." *Pulp and Paper Canada* 77.9 Sept. 1976: 29-33.

Yli-Kaupila, Jouko and Rautpohja Valmet. "How to Improve Wet Pressing." *Paper Technology* June 1993: 29-33.